Boiling vapour-type fluids from the Nifonea vent field (New Hebrides Back-Arc, Vanuatu, SW Pacific): Geochemistry of an early-stage, post-eruptive hydrothermal system

Katja Schmidt[1], Dieter Garbe-Schönberg[2], Mark D. Hannington[3], Melissa O. Anderson[3], Benjamin Bühring[1], Karsten Haase[4], Christy Haruel[5], John Lupton[6], Andrea Koschinsky[1]

[1]Department of Physics and Earth Sciences, Jacobs University Bremen gGmbH, Campus Ring 1, D-28759 Bremen, Germany

[2] Christian-Albrechts-Universität zu Kiel, Institut für Geowissenschaften, Ludewig-Meyn-Str. 10, D-24118 Kiel, Germany

[3] Geomar, Helmholtz Centre for Ocean Research Kiel, Wischhofstr. 1-3. D-24148 Kiel, Germany, and Department of Earth and Environmental Sciences, Universaity of Ottawa, K1N 6N5, Canada

[4]GeoZentrum Nordbayern, Friedrich-Alexander-Universität Erlangen-Nürnberg, Schlossgarten 5, D-91054 Erlangen, Germany

[5]Government of Vanuatu, Dept. of Geology

[6] NOAA Pacific Marine Environmental Laboratory, Newport, OR, USA

Abstract

In 2013, high-temperature vent fluids were sampled at five individual sites in the Nifonea vent field. This field is located within the caldera of a large shield-type volcano of the Vate Trough, a young extensional rift in the New Hebrides back-arc. Hydrothermal venting occurs as clear and black smoker fluids with temperatures up to 368°C, the hottest temperatures measured so far in the western Pacific. The physico-chemical conditions place the fluids within the two-phase field of NaCl-H_2O, and venting is dominated by vapour phase fluids with Cl concentrations as low as 25 mM. The fluid composition, which differs between the vent sites, is interpreted to reflect the specific geochemical fluid signature of a hydrothermal system in its initial, post-eruptive stage. The strong Cl depletion is accompanied by low alkali/Cl ratios compared to more evolved hydrothermal systems, and very high Fe/Cl ratios. The concentrations of REY (180 nM) and As (21 µM) in the most Cl-depleted fluid at NIF-5 are among the highest reported so far for submarine hydrothermal fluids, whereas the inter-element REY fractionation is only minor. The fluid signature, which has been described here for the first time in a back-arc setting, is controlled by fast fluid passage through basaltic volcanic rocks, with extremely high water-rock ratios and only limited water-rock exchange, phase separation and segregation, and (at least) two-component fluid mixing. Metals and

metalloids are unexpectedly mobile in the vapour phase fluids, and the strong enrichments of Fe, REY, and As highlight the metal transport capacity of low-salinity, low-density vapours at the specific physico-chemical conditions at Nifonea. One possible scenario is that the fluids boiled *before* the separated vapour phase continued to react with fresh glassy lavas. The mobilization of metals is likely to occur by leaching from fresh glass and grain boundaries and is supported by the high water/rock ratios. The enrichment of B and As is further controlled by their high volatility, whereas the strong enrichment of REY is also a consequence of the elevated concentrations in the host rocks. However, a direct contribution of metals such as As from magmatic degassing cannot be ruled out. The different fluid end-member composition of individual vent sites could be explained by mixing of vapour phase fluids with another fluid phase of different water/rock interaction history.

1. Introduction

Submarine hydrothermal activity in tectonically active areas at the seafloor provides important pathways for elemental exchange between the lithosphere and the hydrosphere. The oceanic lithosphere acts as both source and sink, and recent studies provide strong evidence for significant net elemental export fluxes into the open ocean through hydrothermal plumes at mid-ocean ridges (e.g., Bennett et al., 2008; Sander and Koschinsky, 2011, Resing et al., 2015). The variability of hydrothermal fluxes and the lifespan of individual hydrothermal systems strongly depend on the tectonic setting, magmatic activity, and seafloor depths. In general, arc and back-arc hydrothermal systems are characterized by higher compositional diversity of venting fluids when compared to mid ocean ridge (MOR) hydrothermal systems (e.g., Manus backarc basin: (Gamo et al., 1997; Craddock, 2009); Mariana arc: (Resing et al., 2007); Valu Fa ridge of the Lau Basin: (Herzig et al., 1998); Kermadec arc: (de Ronde et al., 2005); East Scotia Ridge: (James et al., 2014)). This is related to the increased variability of host rock compositions in arcs and back-arc basins, greater influence of magmatic volatiles, and a larger range of water depths with shallow water depth favouring vapour phase formation during phase separation. The Coriolis Troughs in the eastern part of the southern New Hebrides arc system (SW Pacific) are in a stage of incipient rifting and among Earth's most youthful back-arc basins (McConachy et al., 2005). This setting provides valuable insights into hydrothermal processes linked to initial rifting with near-arc sources of melt supply and unusual alkalic composition of lava flows (McConachy et al., 2005; Anderson et al., 2016).

We here present the results on the fluid chemical composition of Nifonea, including a range of trace metals and metalloids, and He isotopes. As shown below, we were able to sample a backarc hydrothermal system in its initial, post-eruptive stage. Indication for recent magmatic activity comes from very fresh lava, and megaplume events in 2001 and 2004, which are likely related to eruptions (Andersson et al., 2016). This study will add on our understanding of hydrothermal circulation dynamics in youthful back-arc hydrothermal settings with common magmatic activity, and expand the global dataset for hydrothermal vent chemical compositions.

1.1 Geological Setting

The recently volcanically active central chain of the Vanuatu (New Hebrides) arc between 15°S and 21°S stretches from the volcanic islands Ambae and Ambrym in the north to Tanna and Anatom in the south (Fig. 1a; Peate et al. (1997), with a maximum crustal thickness of about 28 km (Ibrahim et al., 1980). Rifting of the island arc started about 3 Ma ago, when the Coriolis Troughs in the south and the Charcot Troughs in the north started forming east of the volcanic islands (Monjaret et al., 1991). The back-arc rifts of the Coriolis Troughs (Vate, Futuna, and Erromango) are at an incipient stage of spreading (Lima et al., (in revision); Price et al., 1993), with volcanic activity in the most active Vate Trough focusing in the Nifonea volcano and its rift zones (Anderson et al., 2016). Hydrothermal precipitates in the Coriolis troughs were first described by Iizasa et al. (1998) who dredged sulphide- and barite-bearing Fe-Si oxyhydroxide deposits in the Futuna Trough and on the rim of a submarine caldera in the northern Vate Trough, and hydrothermal Mn crusts in the Erromango Trough. During the Vanuatu Australia Vents Expedition (VAVE) in 2001, mapping of a 150 m thick hydrothermal plume with methane and manganese anomalies above the Nifonea Ridge in the southern Vate Trough led to the discovery of the active Nifonea vent field, where diffuse venting, extensive hydrothermal fauna, and yellow-brown hydrothermal crusts were observed (McConachy et al., 2005).

1.2 Nifonea vent field

The active, high-temperature hydrothermal vent field “Nifonea” is located in a water depth of 1860–1875 m within a semi-circular caldera, 5 km wide and 8 km long, at the summit of the Nifonea axial volcano in the southern part of the Vate Trough (Fig. 1b). Two volcanic ridges with numerous small volcanic cones up to 50 m high extend from the caldera into the basins to the north and to the south. In the caldera, voluminous fresh, non-sedimented lava flows

were observed indicating recent volcanic activity, megaplume events observed in 2001 and 2004, magmatic eruptions (Andersson et al., 2016). The volcanic features in the vicinity of the hydrothermal field are interpreted as a solidified lava lake of a shield volcano (Lima et al., in revision; Anderson et al., 2016). The composition of the lavas recovered from the Nifonea caldera is transitional from subalkalic to alkalic basaltic to rare andesitic rocks resembling rift magmas enriched in alkalis and incompatible elements such as LREE relative to N-MORB (Lima et al., in revision; McConachy et al., 2005). The youngest volcanic glasses from the caldera interior are significantly more evolved than the older lavas recovered from the caldera rim and flanks of the volcano, which show island arc signatures (Lima et al., in revision).

The vent field with focused high temperature fluid flow occurs in the north of the caldera and consists of three clusters of several small chimneys (<30 cm tall) and few large composite black smoker complexes up to 4 m tall in an area of about 300 m × 300 m. Each high temperature site consists of a small cluster of vents (~20 m × 20 m), surrounded by broken pillows and lobate lava with extensive shimmering water between the pillows and lobes. Vigorous venting of clear fluids was observed from small holes in the brecciated lava with small (<20 cm) chimneys, and from larger chimneys with observable boiling (two-phase behaviour with obvious "flames" of water vapour). The mineralogy of the chimneys is dominated by chalcopyrite indicating high temperatures of mineralization, with minor pyrite, anhydrite and thin rims of Fe-rich sphalerite (Haase and Scientists, 2013). The As sulphides orpiment and realgar were also identified in trace amounts. The absence of any sulphide talus from older, collapsed chimneys indicates a young, initial stage of high-temperature hydrothermal activity (Anderson et al., 2016). Widespread diffuse venting and extensive iron-oxide crusts occur near the main vent field on jumbled and ropey sheeted flows and on pillow mounds emanating from the inter-pillow spaces. This diffuse venting supports patches of mussels and tube worms as well as snails, vent fish, anemones, barnacles and squat lobsters. Some inter-pillow vents within this zone are emitting white fluid and bacterial floc (similar to "snowblower vents" on mid-ocean ridges) that likely contribute to the persistent particle plume that hang over much of the Nifonea caldera (Anderson et al., 2016).

2. Samples and methods

2.1. Vent sites and fluid samples

In October 2010, the *MV Dorado Discovery* surveyed Nifonea using water column sampling methods; and ROV (Remotely Operated Vehicle) dives that recovered sulphide and other rock

samples. High-temperature hydrothermal fluids in the Nifonea vent field were first sampled in July 2013 during the "Coriolis Volcanism and Vents" (COVOLVE) cruise SO229 with the German R/V *Sonne* and ROV *Kiel 6000* (Haase and Scientists, 2013). The fluids were sampled from six individual vent sites in the Nifonea field (named NIF-1, NIF-2, NIF-3, NIF-4, NIF-5, NIF-7); see Fig. 1b, Fig. 2). The actively venting NIF-6 chimney was not sampled for fluids.

Black smoker site NIF-1 was a 2.5 m tall sulphide chimney with numerous small orifices and densely covered with shrimp (Fig. 2a). It is part of a cluster of five up to 4 m tall chimneys. Fluid samples were taken after collapse of the chimney from an open pit in the seafloor (samples 27ROV-14 A, B, C). Although the temperature measurement failed at this site, we can assume exit temperatures well above 250°C (one of the PFA parts was molten, melting temperature >260°C). After 7 days a fresh chimney 20-30 cm tall had regrown and fluids were sampled again (samples 66 ROV-1 see Fig 2b; Tab. 1); one sample was taken from the buoyant plume above the vent (Niskin bottle sample 66 ROV-5). Site NIF-2 is about 150 m to the ENE and comprises few very small vents on the seafloor releasing either greyish or clear fluids (Fig. 2c). One orifice with evidently boiling, clear fluid was sampled (60 ROV-1 B, C, D) at a maximum measured temperature of 345°C. This measured temperature is lower than the predicted two-phase temperature at this depth (~363°C) and might have been due to difficulties in probing the very small focused outlet of boiling fluid with the temperature sensor. Sites NIF-3 and NIF-7 are located in the same vent complex near NIF-1, both was venting black smoke fluids. The fluid sample at NIF-3 was taken after collapse of one of the 3-4 m tall candlestick chimney (66 ROV-6, at 165°C), and NIF-7 was sampled with 66 ROV-3. Within this chimney cluster also boiling fluids were sampled, from chimney site NIF-4 (sample 77 ROV-6), with a maximum measured fluid temperature of 368°C (Fig. 2e). Site NIF-5 occurs halfway between NIF-1 and NIF-2, as a <1 m tall chimney with several orifices (Fig. 2f). Greyish to black venting fluids could be seen to be boiling, again with a maximum temperature of 368°C (sample 77 ROV-10). No fluid samples were taken at site NIF-6. Here, rock samples collected at the base of the chimneys consisted of brecciated volcanic talus highly altered to a clay-rich argillic mineral assemblage and with fractures lined by minor arsenic-sulphides realgar and orpiment.

2.2. Methods

Using the ROV *KIEL 6000* platform, hydrothermal fluids were sampled with the inert and trace metal-clean flow-through fluid sampling system KIPS (Kiel Pumping System, KIPS-4;

(Garbe-Schönberg et al., 2006)). Parallel to the titanium nozzle is a dual channel high-temperature probe (Pt-1000 thermocouple and NTC thermistor sensors, calibrated to 450°C and connected to a RBR logger TBR-2050) delivering online real-time temperature data to guide the ROV co-pilot during fluid sampling. The individual fluid samples are pumped via the titanium nozzle and a PFA tubing into PFA sample bottles. The system is not gas-tight and can hold 2-3 bars. Immediately after recovery of the ROV on deck the KIPS sample rack was transferred to the laboratory for sub-sampling following a standardized protocol. A number of parameters were analysed on-board (see below) and after homogenization, sample aliquots were taken for subsequent analysis in the home laboratories: (i) 20 mL for anions, (ii) 60-125 ml original fluid, not filtered, acidified with 1-5 ml subboiled HNO_3 per 100 ml fluid and stored in PFA bottles, for trace metals; (iii) 60 ml pressure-filtrated (99.9990 nitrogen) through 0.2 µm Nuclepore PC membrane filters in a Sartorius filtration unit, acidified with 0.2 ml subboiled concentrated HNO3 per 100 ml and also stored in 100 ml PFA bottles until analysis. Procedural blanks were processed in regular intervals. All work was done in a class 100 clean bench (Slee, Germany) using all-plastic labware (HDPE, PC, FEP, PFA). Rinse water was ultrapure (>18.2 MOhm) dispensed from the shipboard Sartorius ultrapure water system.

To determine total element concentrations, fluid samples were centrifuged and filtered through 0.2 µm cellulose acetate (CA) filters in the home laboratory. Particles that may have precipitated during or after sampling were then dissolved following a multi-step mixed acid (HF-aqua regia) pressure digestion procedure. The final digest solution was re-homogenized with the fluid filtrate.

Concentrations of major and minor elements (Cl, Br, B, Si, Na, K, Ca, Mg, Sr, Ba, Fe, Mn) were determined by optical emission spectrometry (ICP-OES, Spectro Ciros SOP) after matrix-matched calibration. Analytical error as determined from replicate measurements of samples was <1 rel. % (1 SD). Trace elements (Ge, Al, Rb, Cs, Ba, Fe, Mn, Co, Ni, Cu, Zn, Cd, Ag, Ga, In, Sn, Pb, Tl, As, Se, Sb, Mo, W, U) were determined by both quadrupole-based inductively coupled plasma – mass spectrometry (ICP-MS, Perkin Elmer Elan-5000 in Bremen, Agilent 7500cs in Kiel) and high resolution sector-field ICP-MS (Thermo Element XR in Kiel). Analytical error for the latter techniques was typically <5-10 rel. %. For seawater-like samples, there is only a very limited selection of reference materials. Accuracy was monitored during all analytical procedures with IAPSO seawater (recommended values for major and minor elements: Mg, Cl, Na, K, Ca, Li, Sr, Mo, U), NASS-5 seawater (recommended values for Mo), fresh water NIST-SRM 1643e (recommended values for trace

elements: Al, Sb, As, Ba, Bi, B, Cd, Co, Cu, Fe, Pb, Li, Mn, Mo, Ni, Rb, Se, Sr, Th, V, Zn) and an in-house hydrothermal fluid standard (JUB). We also use artificial seawater with spiked element concentrations in the range as expected for the hydrothermal fluids. The rare earth elements and yttrium (REY) were determined by matrix separation and pre-concentration following the protocol of (Schmidt et al., 2010), and measured with the Perkin Elmer Elan 5000 in Bremen. Ambient seawater was sampled about 15 km NW of the Nifonea vent field, during station 56 CTD at 1900 m water depth.

In October, 2010, three CTD tow-yo hydrocasts CTD-045T, -046T, and 047T were sampled during a survey above the Nifonea hydrothermal field by Bismarck Mining Corporation (Vanuatu) Limited (Neptune Minerals, Inc.) for the investigation of He isotopes. The $^{3}He/^{4}He$ ratio in Earth's mantle is enriched by an order of magnitude above that in the atmosphere, making ^{3}He a uniquely unambiguous indicator of magmatic activity. Because both isotopes of helium are stable and conservative, helium is only removed from the oceanic water column by ventilation into the atmosphere. Thus it is typical for a regional "background" inventory of helium to develop in a basin affected by hydrothermal input of mantle helium. We used helium isotope measurements of nearby water-column plume samples taken in 2010 Bismarck Mining Corporation (Vanuatu) Limited (Neptune Minerals, Inc.) to calculate the $^{3}He/^{4}He$ ratio of the pure hydrothermal end-member fluids from the Nifonea vent field. The water samples for helium isotopes were sealed into copper tubing using a special hydraulic crimping device (Young and Lupton, 1983). In total, 13 samples from 1482 m to 1861 m water depths were selected. Helium isotope ratios were measured at NOAA's Pacific Marine Environmental Laboratory (PMEL) in Newport, Oregon using a dual-collector mass spectrometer designed specifically for helium measurements. The precision for $^{3}He/^{4}He$ measurements was about 0.2 % (1 SD) in $\delta^{3}He$.

3. Results

3.1 pH

The lowest measured $pH_{25°C}$ of 2.9 was determined at site NIF-5, whereas the clear fluid venting at site NIF-2 had a significantly higher pH of 4.7–5.2, possibly due to mixing with up to 50% seawater (see section 3.2).

3.2 Fluid end-member calculation

Measured concentrations and calculated end-member compositions of Nifonea vent fluid samples are presented in Table 2. Dissolved Mg concentrations of Nifonea fluids range from 43.2–3.9 mM Mg, compared to 52.8 mM Mg in ambient seawater. This depletion in Mg concentration suggests that pure end-member fluids from individual vent sites contain zero Mg resulting from quantitative removal of Mg during water/rock interaction (Mottl and Holland, 1978). Based on this assumption, most samples contain 70–93% of the hydrothermal fluid end-member, but a few samples are more diluted due to either entrainment of seawater below the seafloor or during fluid sampling. Using the chemical composition of the ambient seawater sample, fluid endmember compositions were calculated for those vent sites with at least one sample containing >50% hydrothermal fluid. Measured concentrations in fluid samples from the same vent orifice are extrapolated to zero Mg concentration using a linear least squares regression with forcing passage through ambient bottom seawater (ABSW) concentrations (Von Damm et al., 1985). The uncertainty of regression (SD) is generally determined by the minimum Mg content of the fluid samples, by the linearity if the regression trend, and by the measurement uncertainty. Monte-Carlo simulations were used to include an average measurement uncertainty (5% RSD) into the calculation of the uncertainty of regression. This is of special importance for regressions with only one fluid sample. For two of the chimneys (NIF-4 and NIF-5) endmember calculations are based on one fluid sample, while for NIF-1 and NIF-2 at least two samples are used. For NIF-2, this has no effect on the regression uncertainty, which is here dominated by the variance of the individual fluid samples and the Mg content. Calculated end-members based on samples with relatively high Mg concentrations generally have a higher regression uncertainty. We calculated individual fluid end-member compositions for vent sites NIF1, NIF-2, NIF-4 and NIF-5. The calculation of end-member metal concentrations are based on the assumption, that all particles only formed during incipient mixing with seawater prior, during or after sampling (see also Schmidt et al., 2007). As the acid-digested particles in the sample flasks may not always have been homogenously distributed in the sub-samples, metal concentrations have a higher uncertainty.

3.3 Geochemical trends and endmember composition of Nifonea vent fluids

The chemical composition of hydrothermal vent fluids results from water-rock interaction in the subseafloor and processes taking place at the sampling site. Key factors such as temperature, pressure, water-rock ratio, time, mixing of different fluid types, and degree of mixing with cold seawater determine physico-chemical conditions in the fluids and hence

their chemical composition. Several fluid parameters are used to infer p-T conditions (e.g., Cl), to deduce the extent of fluid-rock interaction in the seafloor (Li, Si, Ge/Si ratios, REY inter-element fractionation), to discuss the contribution of a magmatic fluid (As), and to prove fluid mixing (element/Cl ratios) at Nifonea.

The samples of the individual chimneys define different geochemical trends in element-Mg regression graphs (see Fig. 3), resulting in significantly different end-member compositions. A range of composition characterizes the end-member compositions of elements known to behave conservatively during mixing with seawater (such as Cl, Na, Br, K, Li), and these differences can directly be used to discuss subseafloor processes prior to venting. The endmember composition of other elements, however, can easily be modified by sulphide or sulphate mineral formation during mixing with seawater. Individual samples from one chimney hence may display a significant scatter for transition metals such as Cu and Zn in the regression graphs (see NIF-1, Fig. 3), limiting the accurate calculation of end-member concentrations. A discussion of different fluid endmember compositions must thus be handled with caution with respect to these elements. In the Nifonea vent field, the Cl concentrations in the fluids strongly indicate fluid phase separation (see below). As this process overprints the previous fluid-rock history, element/Cl ratios ca be used to evaluate the overall enrichment o depletion of elements relative to seawater. Chloride-normalized elemental concentrations in Nifonea vent fluids are presented in the Electronic Annex, Table EA 2.

3.3.2 Anions Cl, Br

All samples have lower Cl concentrations than ambient bottom seawater (ambient seawater, represented by sample 56 CTD-1900m: 545 mM Cl, 52.8 mM Mg) (Fig. 3). NIF-4 fluids have a relatively high Cl concentration with 259±24 mM, while the other vents all have calculated endmember concentrations of less than 70 mM (NIF-1: 55±11 mM; NIF-2: 66±34 mM; NIF-5: 25±4 mM) Bromide strictly follows chloride, with 387±36 µM for NIF-4, and 59±7 µM at NIF-5, accompanied by an increasing Br/Cl ratio with decreasing endmember Cl (from $1.49*10^{-3}$ to $2.35*10^{-3}$, ambient seawater: $1.47*10^{-3}$). The Cl concentration of the vent fluids provide evidence for phase separation in the subseafloor and the emanation of a vapour phase.

3.3.3 Alkali elements Na, K, Li, Rb, Cs

Sodium, K, Li, and Rb strictly follow Cl and are depleted in all fluid samples relative to seawater, except for Li in NIF-4. The NIF-4 fluid with significantly more Cl relative to the other fluids has highest endmember concentrations of Na (168±19 mM), K (4.67±0.45 mM),

Li (31 mM±2 µM), and Rb (1.03±0.08 µM). In contrast, NIF-5 has the lowest concentrations of Na (21±3 mM), K (0.38±0.07 mM), Li (2.2±0.22 µM), and Rb (0.09±0.02 µM). The measured concentration of Cs in these fluids cluster around ambient seawater at NIF-1 and NIF-2 (1.91-2.4 nM and 2.33-2.39 nM, respectively), which makes an endmember regression impossible. NIF-4, again, has enriched (over sw) concentrations of Cs, with 10±0.6 nM, while NIF-5 only has 0.48±0.03 nM Cs. Relative to seawater with $Li/Cl=0.048*10^{-3}$, Li/Cl in Nifonea vent fluids is enriched. However, this enrichment is small when compared to other hydrothermal systems (Electronic Annex, Table EA 3, Fig. 4). The highest Li/Cl ratio ($0.12*10^{-3}$) occurs at NIF-4. K/Cl is slightly depleted in all fluids relative to seawater (0.015 to 0.20, relative to 0.019 in sw), and Rb/Cl and Cs/Cl are both slightly enriched (Fig. 4). For K, Li, Rb, and Cs, the Cl-normalized ratios are smaller at NIF-5 compared to NIF-4. Na/Cl ratios are slightly depleted at NIF-4 relative to seawater (0.65, relative to a sw ratio of 0.86).

3.3.1 Sulphate

Sulphate is known to be quantitatively removed during water/rock interaction in most hydrothermal systems and, with one exception, the end-member concentrations in the Nifonea vent fluids approach zero SO_4^{2-} (between -1.3±2 mM and 2.1±0.2 mM)**,** consistent with this behaviour. Significant deviations from this trend either results from removal of seawater-derived sulphate in the form of barite or anhydrite during mixing with hydrothermal vent fluids (negative values), or a release of sulphate. At NIF-2, one of the fluid samples has an elevated end-member SO_4 concentration of 10.1 mM, while the more seawater-diluted sample from the same site results in -18 mM SO_4^{2-}.

3.3.4 Alkali earth elements Ca, Sr

Measured Ca concentrations scatter around ambient seawater composition (10.4 mM Ca) in NIF-1 and NIF-2 fluid samples and do not show a trend of depletion or enrichment relative to seawater. Low Ca concentrations are observed at NIF-5 (5.3±0.3 mM), while NIF-4 is significantly enriched, with 35±2 mM Ca in the end-member. A similar distribution is seen for Sr, with lowest end-member Sr at NIF-5 (11.7±1 µM), and highest concentration at NIF-4 (53.6±4.4 µM). Both, Ca/Cl and Sr/Cl are enriched in all fluids relative to seawater (sw: $Sr/Cl=0.17*10^{-3}$, Ca/Cl=0.019); but with strongest relative enrichment in the NIF-5 fluids ($Sr/Cl=0.43*10^{-3}$; Ca/Cl=0.21) and lowest relative enrichments in NIF-4 fluids.

3.3.5 Si, Ge, Al, U, Mo

Silica is considerably enriched in all fluids relative to seawater. Except for NIF-2, samples from the individual sites lie on a similar trends, with end-member concentrations between

4.4±0.16 mM at NIF-1 and 5.6±0.3 mM at NIF4 (Fig. 3). NIF-2 fluids however, show significant scatter in the Mg regression plot, with an average end-member of 8.3 mM Si. Here, the more seawater-diluted sample (which yields negative SO_4^{2-}) would result an apparent end-member concentration of 12.6 mM. Germanium is tightly coupled with Si and enriched in all fluid samples, with 17.6 nM Ge at NIF-1, and 39 nM Ge at NIF-2. The Ge/Si ratios range from seawater-like ratios at NIF-1 ($3.9*10^{-6}$) to slightly elevated ratios at NIF-4 ($5.7*10^{-6}$). Coupled to the relative enrichment of Si and Ge at NIF-2, Al shows highest concentration at this site with 42±3 nM. compared to 1.4±0.05 nM at NIF-1 to 4.4±0.2 nM at NIF-4. Relative to Cl, Si and Ge are most enriched at NIF-4 with lowest end-member Cl (Si/Cl=0.21, Ge/Cl=$1.1*10^{-3}$), and lowest at NIF-5 (Si/Cl=0.02, Ge/Cl=$0.12*10^{-3}$). Aluminium shows the highest Cl-ratios at NIF-2.

Molybdenum and U are known to be insoluble in reducing fluids, and end-member concentrations trend to zero U and zero Mo in most hydrothermal fluids. In the Nifonea fluids, there is a more complex distribution. Uranium is depleted in all fluids and end-members approach zero at NIF-1, NIF-2, and NIF-5, but are higher at NIF-4 (2.9 nM). U/Cl ratios all depleted relative to seawater in at all sites. Molybdenum is also generally depleted in most end-member fluids, but display seawater-like concentrations at NIF-4 (133 nM). Chloride-normalized ratios show an enrichment of Mo relative to seawater at NIF-4 ($0.51*10^{-6}$) and NIF-5 ($0.87*10^{6}$).

3.3.6 Boron

Boron is enriched in the Nifonea fluids relative to ambient seawater (419 µM B), with highest concentrations at NIF-5 (1560±75 µM). B/Cl ratios are higher than in seawater (Fig. 4). Similar concentrations are calculated for site NIF-4 (1420±77 µM). NIF-1 and NIF-2 fluids have end-meber concentrations of 1030-1110 µM B. B/Cl ratios are negatively correlated with end-member Cl concentrations and increase from NIF-4 (B/Cl=$5.5*10^{-3}$) to NIF-5 (B/Cl=$62.3*10^{-3}$).

3.3.7 Transition metals Fe, Mn, Cu, Co, Zn, Ag, Cd, and In, Ga Pb, Sn, Tl

Despite the low Cl concentrations in Nifonea vent fluids, transition metals are strongly enriched in all fluids. At NIF-1, the element concentrations show some scatter in the data, which is partly related to the non-conservative behaviour during seawater admixture. The strongest enrichment of all these elements occurs in the most Cl-enriched fluids at site NIF-4.

Fe and Mn: There is strong enrichment of Fe despite the strong Cl depletion in most end-member fluids, with 1190±45 µM at NIF-1, 7380±390 µM at NIF-4, and 677±33 µM at NIF-

5. Lower Fe concentrations of 174±12 µM are observed in the clear fluid venting at NIF-2. The Fe/Cl ratios are generally very high and range from $21*10^{-3}$ (NIF-1), $28*10^{-3}$ at NIF-4, and to $27*10^{-3}$ at NIF-5, but are only $2.6*10^{-3}$ at NIF-2. Manganese end-member concentrations range from 100±5 µM at NIF-4 to2100±112µM at NIF-4. The Fe/Mn ratio is almost doubled in NIF-5 fluids relative to NIF-4 fluids.

Cu, Co, In: These elements co-vary and have the highest end-member concentration in the Cl-rich fluids at NIF-4, with Cu=32.3 µM, Co=380 nM, In=26.7 nM. However, the strongly Cl-depleted fluids at NIF-5 also have high end-member concentrations, with 9.7 µM Cu, 72 nM Co, and 8.5 nM In. Lowest concentrations occur in the NIF-2 fluids. The solubility of metals such as Co, Cu, In (and Se) in hydrothermal fluids decreases with decreasing fluid temperature (Trefry et al., 1994; Seyfried and Ding, 1995; Metz and Trefry, 2000; Resing et al., 2007; de Ronde et al., 2011), at temperatures <360°C these elements have a preference to be incorporated into Cu-Fe sulphides (Hannington et al., 1995; Seyfried Jr. et al., 1999; Metz and Trefry, 2000).

Zn, Cd, Pb, Tl, Ag, Ga, Sn: These elements also co-vary, with the strongest enrichment in in NIF-4 fluids (Table 2). A number of these elements are preferentially incorporated in Zn sulphides and therefore tend to be removed from the fluids only at low temperatures when Zn sulphides form. Despite similar salinities, Cd, Ga, and Ag are notably enriched in the clear fluid from NIF-2, compared to black smoker fluids from NIF-1. Element/Cl ratios are highest at NIF-4, about 3x more than in NIF-5.

3.3.8 Sulphur group H_2S, As, Sb, Se

Dissolved H_2S shows similar enrichments at NIF-4 and NIF-5, with 6.5±0.34 mM and 6.7±0.35 mM. The clear vent fluids at NIF-2 are characterized by significantly higher end-member concentrations of about 15.1±1 mM H_2S. For NIF-1, individual samples do not follow on a conservative mixing line between fluid and seawater, as one more diluted fluid sample (~50% sw) has higher H_2S concentration than the less diluted one. The calculated end-member based on the less diluted sample is 8.7 mM. The Fe/H_2S ratio is similar at NIF-1 and NIF-5, with 0.10 to 0.11, but significantly higher at NIF-4, with 1.13. Highest H_2S/Cl ratios occur in NIF-5 fluids ($H2S/Cl*10^{-3}$=266, compared to NIF-4 with $H2S/Cl*10^{-3}$=25).

For As, Se, and Sb, we observe different trends at each vent site, regardless of the Cl concentration. NIF-4 and NIF-5 fluids have highest end-member As concentrations (about 21 µM at NIF-4 and NIF-5, which results in much higher As/Cl ratios at NIF-5). NIF-1 fluids have 10±0.3 µM As and NIF-2 fluids 15.1±1 µM. Similar concentrations at NIF-4 and NIF-5

were also observed for B, REY, and H_2S. The concentrations are among the highest ever reported for hydrothermal fluids (Douville et al., 1999; Breuer and Pichler, 2013). In contrast to As, Se (up to 441 nM) and Sb (up to 88 nM) are more enriched in NIF-4 fluids (Se: 442±23 nM; Sb: 88.4±4.7 nM) compared to NIF-5 fluids (Se: 166±8 nM, Sb: 32.3±1.6 nM). Co-varying with the Cu-Co-In group, the lowest Se concentrations occur in the clear NIF-2 fluids (32.2 nM), while the lowest Sb concentrations occur in the black-smoker NIF-1 fluids (14±3 nM).

3.3.9 Rare earth elements and yttrium

The of rare earth elements and yttrium (REY) in Nifonea vent fluids are strongly enriched compared to seawater, and the chondrite-normalized distribution is characterized by an enrichment of LREE over HREE, a positive Eu anomaly (Eu/Eu^*_{CN} = 2.3-3.4), and chondritic Y=Ho, typical of high-temperature hydrothermal fluids. Figure 5 shows end-member REY distribution in Nifonea vent fluids relative to available data for fluids from sediment-starved MOR and back-arc hydrothermal systems, together with the average REE distribution in Nifonea lava from the caldera. The absolute REE concentrations are relatively similar at NIF-2, NIF-4, and NIF-5 and among the highest ever reported for hydrothermal systems (Table 3), but the size of the positive Eu anomaly is relatively small. The LREE/HREE ratio in NIF-4 fluids is lower compared to NIF-5 fluids. The REY/Cl ratio is significantly higher at NIF-5 ($REY/Cl=7.1*10^{-6}$) than at NIF-4 ($REY/Cl=0.44*10^{-6}$).

3.3.10 He isotopes

The highest $^3He/^4He$ ratio measured in the water-column samples was a δ^3He of 99%, or about 2.0 Ra (Electronic Annex, Table EA 1). The slope of a plot of ^3He vs. ^4He concentrations corresponds to the $^3He/^4He$ ratio of the pure hydrothermal fluid, and a linear regression fit to the water-column helium measurements gave a slope of 9.1±0.02 Ra (see Electronic Annex, Figure EA 1).

3.4 Compositional variation within the field

The variation in vent fluid composition is generally linked to the salinity variation. Fluids emanating from the NIF-4 black smoker with 259 mM Cl are characterized by elevated end-member concentrations of alkali and alkali earth elements and Br, the highest content on metals and metalloids such as Fe, Mn, Cu, Zn, Co, Cd, Ag, In, Sn, Pb, Tl, Se, Sb, Mo, and U, and a very high Fe/H_2S ratio compared to the other vent sites with less than 70 mM Cl. In contrast, B, H_2S, and As concentrations are similar in the most Cl-depleted NIF-5 fluids and the most Cl-enriched NIF-4 fluids. Except in NIF-2 fluids, Si and Ge are only slightly

enriched in NIF-4 fluids relative to NIF-5 fluids, whereas REY concentrations are highest in NIF-5 fluids. When comparing the most Cl-depleted NIF-5 fluids and the most Cl-rich NIF-4 fluids, most element/Cl ratios including the volatile B, As, and H_2S, but also Ge, Si, Al, Ca, Br, H_2S, REY and metals such as Cu, Pb, Zn, Mn, Tl are most enriched at NIF-5 (see Figure 4). This results in element/Cl_{NIF-5} / element/Cl_{NIF-4} ratios above one (EA Table 3). The increase in element/Cl ratios from NIF-4 to NIF-5 fluids is in the following order: REY>B>H2S, As, Si, Ge>Al>Cu, Zn, Pb, Tl. In contrast, Li/Cl, K/Cl, Cs/Cl, Li/Rb and Cs/Rb ratios are higher in the Cl-rich fluids at NIF-4 (EA Table 3), whereas Fe/Cl ratios are similar in NIF-4 and NIF-5 fluids.

Hydrothermal fluids venting at NIF-2 are characterized by significant SO_4 concentrations in the calculated fluid endmember, accompanied by enhanced concentrations of Si, Ge, Al, and H_2S (for more detailed discussion see chapter 4.3).

4. Discussion

4.1 Processes in the sub-seafloor

4.1.1 p-T conditions of phase separation

The individual end-member fluids are characterized by different Cl concentrations. The water depth of the Nifonea vent field corresponds to a pressure of 188–189 bars, which places the hottest fluids with 368°C into the 2-phase field of the system NaCl-H_2O, close to the two-phase boundary of seawater (Fig. 6). The characteristic flame-like appearance of venting fluids, observed at the at the vent sites NIF-2, NIF-4, and NIF-5 (Fig. 2), is a visual evidence for *in situ* boiling. The flame is produced by low-density vapour that condenses rapidly due to cooling and mixing with surrounding seawater. The extreme Cl depletion in these fluids (end-member lowest Cl end-member = 25 mM) relative to ambient seawater (545 mM Cl) confirms venting of vapour phase fluids.

The Cl concentration in co-existing vapour and brine phases at given p-T conditions can be calculated, based on phase relations in the pressure-temperature-composition (p,T,X) space for NaCl-H_2O. At Nifonea, the p, T conditions are ~188 bars and 368°C; therefore, corresponding to predicted Cl concentrations of 3 to 5 mM in the vapour during equilibrium partitioning (SoWat program, (Driesner, 2007; Driesner and Heinrich, 2007), which is lower than the lowest calculated endmember Cl concentration of 25 mM at NIF-5. The corresponding brine phase would have 2250 mM Cl. While phase separation at greater depths

would yield higher Cl (e.g., 30 mM Cl at 2200 m depth, 380°C), this salinity would only be preserved if the ascent of a segregated vapour phase to the seafloor occurs in the single-phase field. This, however, is not consistent with the maximum temperatures of 368°C determined during fluid sampling at NIF-4 and NIF-5. A simple calculation shows, that only ~1.4 vol. % of a brine previously segregated from the vapour, with a Cl concentration of 2250 mM Cl, is required to increase the vapour phase Cl concentration from 3 mM to ~ 30 mM. About 11 vol. % of the brine phase increases the Cl content to 259 mM Cl, the calculated end-member concentration for NIF-4. While this could explain the observed salinities at the different vent sites, variable element/Cl ratios (Figure 4) strongly argue against a simple mixing model for the different sites. Generally, alkali/Cl and alkali earth/Cl ratios should be unaffected by sub-critical phase separation at p-T conditions similar to Nifonea (Von Damm et al., 1985; Von Damm, 1990; Berndt and Seyfried, 1990; Ogawa et al., 2005; Foustoukos and Seyfried, 2007b), and a variation in element/Cl ratios between fluid end-members as observed in the Nifonea vent field (see chapter 3.4) must be controlled by processes/conditions other than phase separation and re-mixing of vapour and brine being segregated before. The different end-member fluids either result from independent fluid circulation, phase separation, and (re)mixing below each vent site, or they result from mixing at variable proportions of at least two different fluid types with different water-rock interaction and phase separation history in the subseafloor. In this case, a pure vapour phase is mixed with another high-temperature fluid phase prior to ascent, which may have been either "evolved" seawater (i.e., Mg-free, not phase separated, limited water-rock interaction) or a brine phase, originating from deeper in the hydrothermal plumbing system and with a different water-rock interaction history. A third possibility is that this fluid is a condensed vapour phase generated deep in the crust (with relatively high Cl content), which raises to the seafloor in the single-phase state. However, other observations such as high water-rock ratios with limited water-rock exchange argue against a deep-circulating fluid at Nifonea (see discussion below).

All fluids are characterized by a depleted Na/Cl ratio relative to seawater, with lowest values at NIF-4 and highest values at NIF-5. The Na depletion likely results from uptake during albitization in the subseafloor,

4.4.2 Depth and extent of water-rock interaction

4.4.2.1 Depth

To constrain pressure-temperature conditions of high-temperature reaction zones, different approaches are available and will be critically discussed below. Silica concentrations in hydrothermal fluids are assumed to be controlled by the p-T-dependent solubility of quartz in

512 the host rocks (Von Damm et al., 1991), and can used to estimate the depth of the high-
513 temperature reaction zone. Although the quartz solubility is poorly constrained at the p-T
514 conditions of Nifonea, an equilibrium depth of well below 250 bars (i.e., not deeper than a
515 few hundred m below the seafloor) is indicated at temperatures measured during fluid exit. At
516 higher temperatures above 390°C, higher equilibrium pressures are possible (e.g., 410°C/300
517 bars). However, in a hydrothermal system with fast fluid passage through the rocks, with
518 limited water-rock interaction, Si concentrations in the fluid may not be controlled by
519 equilibrium conditions.
520 Fousoukos and Seyfried (2007a) and Fontaine et al. (2009) use the quartz-fluid phase
521 equilibria for the two-phase NaCl-H_2O system, independent of measured exit temperature. By
522 applying this approach with measured Cl and Si concentrations at NIF-4 and NIF-5,
523 temperatures >400°C and a deep reaction zone (>280 bars) could be deduced (NIF-5:
524 >415°C/>290 bars (Fontaine et al., 2009), 420-430°C/~280 bars (Foustoukos and Seyfried,
525 2007a; NIF-4: ~400°C/~280 bars (Fontaine et al., 2009), 400-410°C/~290 bars (Foustoukos
526 and Seyfried, 2007a)). However, there is one shortcoming with this approach: it implies that
527 Cl and Si concentrations did not change during fluid ascent. The hypothetical equilibrium T
528 and p of NIF-5 place the fluid in the two-phase seawater. Chloride concentrations change with
529 changing depth when travelling in the two-phase field due to re-equilibration, and a
530 concentration of 25 mM Cl generated deep in the subseafloor would only be preserved when
531 fluid ascent occurs in the single-phase field. However, p-T conditions measured at NIF-5
532 during fluid exit place the fluid into the two-phase region, which has also visually been
533 observed. Si kinetics in contrast are slow and Si would not change and could thus inherit
534 signal from deeper in the crust. Besides this, phase equilibria of quartz are also poorly
535 constrained for the measured Cl concentrations measured at NIF-5 (outside the range of
536 experimental data) and given p-T ranges have high uncertainites. At conditions below 235
537 bars and 390°C, equation used to predict quartz solubility not valid (Foustoukos and Seyfried
538 2007a). Another approach to reconstruct p-T conditions in high-temperature reaction zones
539 uses the Fe/Mn geothermometer of Pester et al (2011). The Fe/Mn ratios of about 6.7 at NIF-
540 5 and of about 3.5 at NIF-4 correspond to equilibrium temperatures of 400-420°C and 380-
541 400°C, respectively. Again, this approach has its limitations, and caution is necessary with
542 fluids <200 mM Cl, as Fe preferentially partitions into vapour relative to Mn (Pester et al.,
543 2011, Pester et al., 2014).
544 The above-mentioned approaches show that a situation with a deep reaction zone more than
545 1km below the vent field, with fluid temperatures above 400°C, cannot be ruled out.

However, the balance of observations, such as ongoing magmatic activity, He isotopes (see section 4.4.2.2), high w-rock ratios indicating quick fluid passage with limited water-rock interaction (see section 4.4.2.3) rather argue for shallow reaction, with diking events delivering heat very shallow into the crust. Fluid passage likely occurs within the young, glassy lava, an interpretation suppored by He isotopes data. The younger Nifonea lavas were formed from a more enriched, MORB-type mantle source compared to the older lavas from the caldera flank displaying subduction signatures.

4.4.2.2 Helium isotopes

Helium isotopes have been shown to be a useful geochemical tracer for distinguishing between depleted mantle or mid-ocean ridge (MOR-type) and fertile (hotspot) mantle sources. The $^{3}He/^{4}He$ endmember ratio of 9.1R/R_a calculated from water samples above the Nifonea vent is at the upper end of the range that might be expected for spreading centres with ^{3}He predominantly sourced from depleted upper mantle: MORB and hydrothermal systems hosted therein cluster at R/R_a= 7-9 (Lupton et al., 2009; Ishibashi et al., 2015), while submarine arc/backarc hydrothermal fluids sourced from depleted upper mantle such as Valu Fa Ridge in the Lau Basin typically have $^{3}He/^{4}He$ = 7.5-8.5 (Fourre et al., 2006; Takai et al., 2008; de Ronde et al., 2011; Lupton et al., 2015; Ishibashi et al., 2015). In contrast, elevated He isotope ratios in the Manus spreading centre ($^{3}He/^{4}He$ = 12R/R_A; Fourre et al. (2006)), the northwest Lau backarc basin ($^{3}He/^{4}He$ = 10.6 up to 18.7R/ R_A, Lupton et al. (2012)) and in the North Fiji Basin ($^{3}He/^{4}He$ = 9.8R/R_A; Ishibashi et al. (1994), Zeng et al. (2015)) are thought to reflect significant contribution from a lower (fertile) mantle component (^{3}He-rich hotspot component). The He isotope ratio of the Nifonea vent fluids is consistent with an upper mantle component and supports the hypothesis that the hydrothermal system incorporated ^{3}He from the young lavas rather than from older subduction-related lavas. Recent work by Jean-Baptiste et al. (2015) on He isotopes in volcanic gases and thermal waters along the Vanuatu volcanic arc show $^{3}He/^{4}He$ ratios of 6.4 - 7.2 R_a at islands fed by Pacific mantle source, which are typical for subduction-related volcanic arcs. Typical MORB values of 7.6 to 8.0 R_a were found on islands fed by Indian MORB mantle. Enhanced ratios of 9.8-10.2 at Ambrym, however, indicates the involvement of a ^{3}He-rich hotspot component influencing the MORB mantle below. The relatively high $^{3}He/^{4}He$ in the Nifonea fluids compared to other back-arc hydrothermal systems complements the observation that the younger lavas in the Nifonea caldera evolve towards more enriched compositions and

represent increasing contributions from an enriched mantle source (Lima et al., in revision), possibly a hot spot component.

4.4.2.3 water-rock ratio

To get an idea about the extent of water-rock interaction, we used a simplified mass ratio calculation. The concentrations of fluid-mobile elements such as Li, Rb, and Cs (and to a lesser extent K) are primarily controlled by their concentration in the rocks, the extent of previous rock alteration, and the water/rock ratio. While K often is affected by secondary mineral formation during rock alteration (which may even result in $K/Cl_{Fluid}<K/Cl_{SW}$ – see below), Li, (and to a lesser extent Rb and Cs) are conserved and hence, good indicators for the extent of water/rock interaction and often used to calculate effective water/rock ratios (Von Damm et al., 1985). Lithium concentrations in fresh Nifonea volcanic rocks are similar to abundances in MORB (5–10 ppm), whereas Rb (15–22 ppm) and Cs (0.18–0.3 ppm) are more enriched (Lima et al., in revision; McConachy et al., 2005). Caesium is enriched in the fluids and the Rb/Cs ratios in the fluids are similar to those in the fresh volcanic rocks, whereas the Li/Rb ratio in the fluids (1.7-2.5) is enriched by a factor of 3 relative to the rocks (~0.4), and slightly enriched relative to its seawater ratio (~1.4). This indicates either that Li is more effectively leached from the rocks or, that Rb and Cs are involved in secondary minerals. Assuming a 100% extraction efficiency of Li, Rb, and Cs from the rocks, access to fresh rock surfaces, no incorporation into secondary alteration minerals and no fractionation during phase separation, the minor enrichment of Li over seawater (as Li/Cl) indicate extremely high water/rock ratios.

The mass ratio of water:rock is calculated in the following way: the rock concentration is divided by the net addition to the fluid (i.e., reduced by seawater concentration). If we assume that phase separation occurred after water-rock interaction, the Cl concentration in the fluid can be corrected for the phase separation effect using the Li/Cl ratio). Using average Li and Cs concentrations of fresh Nifonea volcanic rocks (7 mg/kg and 0.2 mg/kg, respectively) and ambient seawater concentrations (26.5 µM and 1.9 nM, respectively), the calculated water/rock ratio is about 55 for Li, and 200 for Cs. In the NIF-4 fluids with higher Cl concentrations (259 mM Cl) and lower element/Cl ratios calculated water/rock ratios are 25, for Cs 80. There are some limitations to this approach: It might well be that significant interaction with the host rock took place *after* phase separation. In this case the above calculation with its correction to seawater Cl cannot be used. Instead, one would calculate a ratio of volume of vapour reacted with a given mass of rock. Considering the density of the

vaopour (i.e., ~125 kg/m^3 at p-T conditions at Nifonea), this results in a mass ratio of about 120 for NIF-5.

Potassium is depleted relative to seawater, which indicate incorporation into the rock (similar to Na). While most hydrothermal fluids have K/Cl ratios larger than seawater, a depletion is very rarely observed and seem to be a unique signature of early-stage hydrothermal circulation ($K/Cl_{Fluid}<K/Cl_{SW}$: 9°46,5N, Aa vent, , also 9°-10°N, EPR, Von Damm et al., 2000).

Limited water-rock interaction is also indicated by the Si/Ge ratios in the fluids. Silica and Ge are extracted during high temperature seawater/basalt interaction leading to elevated Si and Ge concentrations and Ge/Si ratios when compared to seawater (Ge/Si = 0.72 µmol/mol) and basaltic crust (2.6 µmol/mol) (Wheat and McManus (2008), and references therein). While cold fluids from basaltic host rocks have a slightly elevated Ge/Si of 4 due to incorporation of Si in secondary minerals, this greatly increased in warm (>25°C) ridge flank hydrothermal fluids with Ge/Si = 15-62 µmol/mol (Wheat and McManus, 2008). The Ge/Si ratios in the Nifonea fluids (4-5.7) are at the lower end of reported Ge/Si ratios of 5-15 in high-temperature (350°C) hydrothermal fluids, with an average Ge/Si ratio of 9 (Mortlock et al., 1993; Wheat and McManus, 2008, Escoube et al., 2015) and only slightly elevated relative to basaltic crust average. Both Si and Ge concentrations are strongly increased relative to seawater, i.e., their fluid concentrations are related to mobilization from the host rock. The low Ge/Si ratios in Nifonea vent fluids, with only slight enrichment of Ge relative to Si compared to the host rock, are likely a consequence of high water/rock ratios preventing significant formation of secondary alteration minerals. Formation of secondary silicate minerals would lead to increasing Ge/Si ratios in the fluids, related to discrimination of Ge relative to Si (Mortlock et al., 1993). When the Ge/Si ratio in the fluid is buffered by quartz in the reaction zone (which would also increase Ge/Si in the fluid, as Ge does not partition into the quartz), the relatively low Ge/Si in Nifonea fluids may then be an indication that Si concentrations are not controlled by quartz solubility.

4.1.3 Fluid mixing

The above observations indicate a hydrothermal system with quick fluid passage with limited water-rock interaction and phase separation, likely related to ongoing magmatic activity.The differences in element/Cl ratios of “conservative” elements between individual vent sites and the generally higher metal/Cl ratios in the Cl-poor vapour phase argue against the simple re-

mixing of variable proportions of segregated vapour and brine in a closed system. NIF-1 and NIF-4 are within the same chimney complex, whereas NIF-5 is located about 70 m ENE from NIF-1. NIF-2 is located at the rim of the active vent site, about 30 m NE of NIF-5. To test whether all fluid compositions could be explained by mixing of two components to variable degrees, we plotted the calculated end-member concentration of individual elements from the different vent orifices to their calculated end-member Cl concentration (Figure 7). Endmember black smoker fluids of NIF-1, NIF-4, and NIF-5 seem to plot on a single mixing line between a low-Cl vapour phase of probably ~ 3 mM Cl (see section 4.4.1), and a high-Cl phase of unknown chlorinity, for elements known to behave conservatively during mixing processes (like Na, Br, K, and Rb, Figure 7). This suggests that mixing between two fluid phases could be responsible for the observed variability between the individual smokers at Nifonea, at least for NIF-1, NIF-4, and NIF-5. At NIF-4 with highest Cl end-member concentrations, U is not completely removed, and Mo is even enriched relative to seawater. As in evolved hydrothermal systems the concentration of both elements tend to zero, this argues for a very limited water-rock exchange also for the high-Cl fluid phase and make a deep-seated reaction zone unlikely. The clear fluids of NIF-2 plot outside the conservative mixing trend, which may be related to the specific situation at this site (see section 4.3). Alternatively, individual fluids with different water-rock interaction/phase separation, fluid mixing history may ascent at the individual vent sites. While NIF-5 represents an almost pure vapour phase, the fluid composition of NIF-4 fluids requires substantial (re-mixing) of vapour and brine or evolved seawater.

4.2 Mobility of trace metals and metalloids in the Nifonea vapour phase fluids

Metals and metalloids (M) in the Nifonea vent fluids are unexpectedly mobile in the low-density low-salinity vapour phase fluids venting in the Nifonea vent field, especially at NIF-5. The concentrations of As and REY in NIF-5 fluids, in particular, are among the highest observed so far in submarine hydrothermal fluids (Table 4). Only a few studies of vent fluids provide comprehensive data for all trace metals and metalloids that can be compared with the Nifonea vents. Important exceptions are studies by Douville et al. (2002), Schmidt et al. (2007), Schmidt et al. (2011) on the Rainbow, TAG, and Logatchev fields on the Mid-Atlantic Ridge, by (Metz and Trefry (2000) and Seyfried et al. (2003) on the Main Endeavour Field and two fields at Cleft segment on the Juan de Fuca Ridge, and by Craddock (2009) on various fields in the backarc Manus Basin. Compared to these studies, the generally

significant metal transport in the low-Cl vapour phase fluids at Nifonea is striking. Trace element data are of relevance not only for a better characterisation of young back-arc hydrothermal systems, but also for our understanding of processes controlling their enrichment in massive sulphide ore deposits. Ongoing fluid-rock interaction of the separated vapour with fresh lava in the Nifonea caldera *after boiling* is one possible mechanism responsible for the enrichment of these elements (Table 4, Table EA 2, Table EA 3). The enhanced M/Cl ratios of most of these elements in the NIF-5 fluids relative to the more Cl-rich NIF-4 fluids further provide evidence for the different water-rock interaction history of the (at least) two hypothetical fluid phases mixed prior to venting at Nifonea.

4.2.1 Iron

Iron is very effectively leached from the rocks under the conditions at Nifonea. Even the most Cl-depleted vapour phase fluid has a Fe/Cl ratio of 26×10^{-3}. Similar remarkable Fe enrichments in strongly Cl-depleted fluids relative to other transition metals such as Mn are known from high-temperature MOR fluids venting immediately after a magmatic event, such as at 9°46'46.5"N on the East Pacific Rise (e.g., Aa vents with Fe/Cl = 24×10^{-3}; Von Damm, (2000), Table 4). Such high Fe solubility in low salinity and low-density fluids and increased Fe/Cl ratios relative to single phase fluids have been reproduced experimentally by Pester et al. (2014) and (Foustoukos and Seyfried, 2007a), who attributed the enhanced Fe mobility in low-density Cl vapours relative to Mn and other transition metals to the tendency of Fe to form stronger aqueous complexes than other first-row transition metals. It should be noted, however, that in the experiments by Pester et al. (2014), Fe still partitions preferentially into the brine during phase separation. The experimental evidence confirms the generalized model for the evolution of fluid chemistry in response to seafloor eruptions by Butterfield et al. (1997), which involves phase separation and preferential venting of the more buoyant vapour phase triggered by a greatly increased heat flux immediately following a volcanic eruption. Associated with these initial vapour-dominated fluids are enhanced volatile fluxes (e.g., H_2S, H_2, CO_2) and strongly increased Fe fluxes. One possible explanation is that the post-eruptive fluids mobilize Fe from grain boundaries and interstitial glassy material in fresh lava with greater efficiency despite the low Cl and low density of the fluids. A limited formation of alteration minerals likely further support the enrichment of Fe in the fluids. In this case, both the physico-chemical conditions and the availability of leachable Fe are the main control on the Fe mobility.

4.2.2 REY

The distribution of REY in the hydrothermal fluids provides useful insights into water/rock interaction, in particular the degree of fractionation of selected REY, and the size of a Eu anomaly. The Nifonea vent fluids have among the highest reported REY concentrations in seafloor vent fluids (up to~180 nM), with the highest concentrations in the most Cl-depleted fluid of NIF-5. The REY/Cl is much higher in the low-salinity vapour phase relative to the more Cl-enriched vapour (about 14 times more), which is even more than B, As, Si, Ge (9–11 times higher in NIF-5 relative to NIF-4, see EA table 3).

When normalized to the REE concentration of the young Nifonea lava, the vent fluids display an enrichment of LREE over HREE, a positive Eu/Eu* anomaly, and chondritic Y_N=Ho_N, with a pattern similar to that of high-temperature fluids in mafic or ultramafic rock environments at MOR spreading centres and in evolved back-arc settings. However, the degree of LREE/HREE fractionation, and the size of the positive Eu anomaly are smaller than for MOR hydrothermal systems, consistent with the LREE-enriched lava (Fig. 5).

Hydrothermal leaching experiments by Giese and Bau (1994), Bau et al. (1998), Bach and Irber, (1998), Allen and Seyfried (2005), and Shibata et al. (2006) have shown that LREE are more easily mobilized relative to HREE from basaltic to andesitic rocks, and preferentially leached from late-stage interstitial glassy material and grain boundaries. Fractionation between LREE and HREE is due to the stronger dissolved complexes of LREE with Cl. Incorporation into alteration minerals may further enhance the enrichment of LREE over HREE and can explain the larger Eu anomalies, as neighbouring trivalent REE are preferentially incorporated into secondary alteration minerals such as chlorite and smectite (Bau, 1991; Allen and Seyfried, 2005; Tertre et al., 2008). Results of recent hydrothermal experiments under sub- and super-critical conditions with seawater and natural basaltic to gabbroic material (Beermann et al., 2017) show that the water/rock ratio also exerts a major control on REY distribution. High water/rock ratios >10 establish conditions where REY are rapidly leached and readily dissolved without re-incorporation and fractionation of HREE during the formation of secondary alteration minerals. Fluid REY patterns from these high water/rock experiments mimic the pattern of the host rock with only slight relative enrichment of LREE and Eu (Beermann et al., 2017). This most likely explains the limited incorporation of REE into alteration minerals at high water/rock ratios at Nifonea. The significantly higher REY/Cl ratios at NIF-5 relative to NIF-4 underline the high mobility of REY in low-density vapours (possibly as neutral hydroxo complexes) and is one of the major outcomes of this study.

4.2.3 As and B

As/Cl (770) and B/Cl (58) ratios in the most Cl-depleted vapour phase fluid are significantly higher than in the most Cl-enriched vapour phase fluid of NIF-4 (As/Cl = 80 and B/Cl = 5). End-member concentrations of B and As are similar in both fluid types, which has also been observed for H_2S.

Arsenic concentrations of up to 20 μM are among the highest yet reported in high-temperature submarine hydrothermal fluids, similarly high concentrations were previously only reported from back-arc basin settings with acidic host rocks (Price et al., 1993; Trefry et al., 1994; Douville et al., 1999; Metz and Trefry, 2000; Craddock, 2009; Breuer and Pichler, 2013). The As/Cl ratios in Nifonea vapour phase fluids are about 30 times higher compared to Cl-enriched hydrothermal fluids leaching dacitic rocks with comparably high As concentrations (such as Pacmanus vent field; (Craddock (2009)). Three different processes could be responsible for this remarkably strong enrichment: (1) enhanced fractionation into the vapour phase during phase separation and increased mobility of As in low-Cl, low density vapours, (2) direct contribution of these elements from magmatic degassing, and (3) preferential mobilization at prevailing physico-chemical conditions from rocks, which are potentially enriched in these elements.

Both As and B are known to behave volatile, and fractionation into the vapour phase during phase separation is known from experiments (Heinrich et al., 1999; Pokrovski et al., 2005; Foustoukos and Seyfried, 2007b; Pokrovski et al., 2008). The strong volatile behaviour has been attributed to the formation of uncharged aqueous species, namely $B(OH)_3^0$ and the arsenite species $H_3AsO_3^0$ in low salinity, low-density vapours (Heinrich et al., 1999). However, the fact that high As concentrations are only known from back-arc basin and island arc vent fluids including Nifonea, argues for a special situation in subduction-related environments and shows that phase separation processes alone are not sufficient to explain the enrichment of As (Douville et al., 1999; Breuer and Pichler, 2013).

Direct contribution of As from magmatic degassing cannot be ruled out, and has previously been suggested for other back-arc hydrothermal systems (e.g., Manus Basin; Craddock (2009); Reeves et al., 2011) and ancient porphyry and epithermal deposits (Heinrich et al., 1999; Williams-Jones and Heinrich, 2005).

Although subduction-influenced magmas often contain higher contents of As than MORB, this enrichment alone would not be sufficient to explain the high As concentrations in back-arc basin fluid including Nifonea fluids. There are no data are available yet for concentrations

783 of volatile elements such as As and B in the Nifonea volcanic rocks. There are also no As or
784 B concentration data for post-eruptive East Pacific Rise (EPR) vent fluids at 9°C nor Main
785 Endeavour Vent Field (MEF) fluids with similarly low Cl concentrations, which would allow
786 to evaluate the influence of the host rock on the concentration of volatile elements.
787 We here suggest that the extremely high As concentrations are most likely related to a
788 strongly increased mobility in the low-Cl and low-density vapour due to its volatility, possibly
789 combined with preferential leaching at high water/rock ratios, similar to REY and Fe (As is
790 easily mobilized from grain boundaries, As also substitutes for Fe in silicates). An indirect
791 influence of magmatic volatiles on the mobility of As in back-arc hydrothermal fluids, related
792 to an increased acidity of fluids, may be possible, but cannot be proven. The low pH of about
793 3 might be an indication for a contribution of magmatic volatiles.
794
795 Besides the strong enrichments of Fe (relative to Cl), REY and As, also Zn, Tl, Pb, Cd show
796 metal/Cl ratios in NIF-5 fluids, which are among the highest reported so far for hydrothermal
797 fluids. Continued leaching of the fresh lava by the vapour after segregation from the brine
798 likely explains this enrichment and would be in agreement with experimental evidence
799 (Foustoukos and Seyfried, 2007b; Pester et al., 2014; Pester et al., 2015).

800 ***4.3 Previous hydrothermal activity at Nifonea?***
801
802 At NIF-2, three fluid samples were taken, two with about 22% end-member fluid and one
803 with 53% end-member fluid. While one the more diluted samples has only been measured for
804 major elements, the other two were measured for all elements on interest. Figure 3 shows, that
805 some elements, such as Si, Al (also Ca, Ba, some metals such as Cu, Zn, Ga), don't show a
806 single mixing line. This is accompanied by a non-conservative depletion of SO_4^{2-} in this
807 sample and seem to be related to mineral removal/mineral enrichment processes during
808 mixing with seawater. Sulphate may be removed in form of alunite, as Al is depleted as well
809 (relative to the less-diluted sample). As the calculated end-members using both samples are
810 indistinguishable from the calculated end-members based only on the less diluted sample
811 (within SD, see table 2b), we decided to use the first end-member anyways.
812 The significant sulphate concentration in one of the fluid samples at NIF-2, accompanied by
813 strong enrichment of Al, indicate differences in sub-seafloor water/rock interaction processes
814 close to the venting site, in comparison to the other vent sites, or entrainment of sulphate
815 particles. Positive sulphate endmember concentrations due to anhydrite or barite entrainment
816 and dissolution can be excluded, as whether Ca nor Ba are unusually enriched. We rather

817 suggest a direct or indirect signal from magmatic volatiles: Disproportionation of
818 magmatically-derived SO_2 during fluid ascent and cooling results in formation of SO_4^{2-}- and
819 H^+. Subsequent interaction of the highly acidic fluids with altered mineral assemblages in the
820 upflow zone is assumed to mobilize Si, Fe, and Al (Resing et al., 2007; Seewald et al., 2015)
821 and leads to venting of highly acidic (pH<1), SO_4-rich low temperature fluids enriched in Si
822 and Al. These so-called acid-sulphate type magmatic-hydrothermal fluids commonly occur in
823 subduction-related tectonic settings, such as the Manus backarc basin (Gamo et al., 1997;
824 Craddock, 2009; Seewald et al., 2015), the Mariana arc (Resing et al., 2007), the Valu Fa
825 ridge of the Lau basin (Herzig et al., 1998), and along the Kermadec arc (de Ronde et al.,
826 2005; de Ronde et al., 2011). The overall similar fluid chemistry compared to the other vents
827 and the moderate pH of 4.7–5.2 argues against a direct contribution of magmatic volatiles.
828 Enriched sulphate and Al concentrations could also derive from the dissolution of alteration
829 minerals such as alunite. Alunite-group minerals $(Na,K)Al_3(SO_4)_2(OH)_6$ and smectite form
830 during argillic alteration due to strongly acidic magmatic-hydrothermal fluids. Reaction of
831 hydrothermal fluids with these alteration minerals would result in a strong increase of Al,
832 SO_4, and Si in the fluid, as observed at NIF-2. Argillic mineral assemblages were indeed
833 observed in a strongly altered rock fragment recovered together with sulphide chimney
834 fragments at NIF-6, about 100 m NW of the NIF-2 site. The main alteration mineral phase is
835 smectite.
836 While ongoing eruptive volcanic activity is indicated by recently erupted, fresh lava in the
837 Nifonea vent field, this altered rock piece and the fluid composition at site NIF-2 may be an
838 indication of previous magmatic-hydrothermal activity in the area pre-dating the current
839 hydrothermal activity. The very low Fe contents and very low Fe/Mn and Fe/H_2S in the clear
840 fluids of NIF-2 suggests that Fe is depleted in the argillic alteration zone from previous
841 reactions. Other metal concentrations such as those of Cu, Co, In, Zn are also low, but these
842 elements are not as depleted as Fe. An alternative explanation involves precipitation of Fe
843 sulphides (pyrite, pyrrhotite) in the sub-seafloor due to seawater mixing or pH increase by
844 reaction with wall-rock, favoured by high H_2S concentrations in the fluids.

845 ## 5. Conclusion

846 The Nifonea hydrothermal field in part vents the hottest (368°C) hydrothermal fluids
847 observed so far in the W Pacific. The vent field probably represents a very young, early-stage
848 hydrothermal system that is associated with very recent magmatic activity. This interpretation

849 is supported by the absence of any sulphide talus from collapsed older chimneys and the very
850 fresh appearance of the surrounding lavas (Anderson et al., 2016).
851 The most Cl-depleted endmember at NIF-5 (<30 mM Cl) represents an almost pure vapour
852 phase at the prevailing p-T conditions of the vent site. Vapour phase fluids with similar low
853 chlorinity were previously only reported from EPR, 9°46'5"N (Von Damm et al., 1995; Von
854 Damm, 2000); EPR 9°50'3"N (Shanks, 2001; Von Damm, 2004; Fornari et al., 2012), EPR
855 9°17'N (Von Damm, 2000) and from the Main Endeavour Field (MEF) at the Juan de Fuca
856 Ridge (Seyfried et al., 2003). The venting of vapour phase fluids at these sites has been
857 related to directly preceding magmatic events. The initial post-eruptive vapour-stage fluids
858 evolved to steady state Cl-normal fluids after some months, accompanied by decreasing Fe/Cl
859 and increasing alkali element/Cl ratios (Von Damm, 2000; Seyfried et al., 2003; Fornari et al.,
860 2012; Yücel and Luther, 2013). The extremely Cl-depleted fluids of Nifonea and EPR
861 9°46'5"N.5'N (Aa vent; Von Damm (2000)), in particular, share several specific
862 characteristics (Table 4), such as minor enrichment of alkali elements relative to seawater,
863 high Fe/Cl and B/Cl ratios and low Si concentrations. Together with the strong enrichment of
864 REY with only minor REY inter-element fractionation, this can be related to rapid fluid
865 passage through host rocks very shallow in the crust, consistent with only limited water/rock
866 interaction with mafic rocks at extremely high water/rock ratios, likely at non-equilibrium
867 conditions. Fluid-rock reaction under very high water/rock ratios causes leaching of the host
868 rocks with only minor changes of compositional patterns of the host rocks, rather than
869 elemental fractionation as a consequence of secondary mineral formation. One likely scenario
870 at Nifonea is that heating of seawater occurs fast and shallow in the crust, and when the
871 critical temperature is reached, boiling occurs. Significant water/rock interaction probably
872 occurred *after boiling*, with the separated vapour phase effectively leaching easily accessible
873 metals from fresh volcanic glass and grain boundaries at high water/rock ratios. In particular,
874 elements with high volatility (As, B) and easily leachable metals such as REY and Fe are
875 mobilized into the vapour phase fluid. Prior or during venting, this vapour phase mixes with
876 various amounts of another fluid, reflected in the different salinities and element/Cl ratios at
877 the individual vents. Whether this is a non-phase separated fluid, which has not yet reached
878 the temperature to boil, a brine phase or a vapour phase formed deep in the crust close to the
879 critical point of seawater, we don't know. However, the latter is not very likely, considering,
880 that the low Li enrichment indicates high water-rock ratios, which is not expected for a fluid
881 circulating deep in the crust. Furthermore, the incomplete removal of U and the enrichment of
882 Mo relative to Cl at NIF-4 argues against equilibrium conditions during water-rock interaction

for the Cl-enriched fluid phase. An individual fluid circulation at each vent site is also possible, but not very likely. The vent sites NIF-1 and NIF-4 occur very close together, within the same chimney complex. An influence of magmatic volatiles, adding elements such as As to the fluids, can also not be ruled out.

The fluid characteristics are interpreted to reflect the specific geochemical fluid signature of a hydrothermal system in its initial post-eruptive stage, described here for the first time in a backarc setting. Similar hydrothermal sites are likely to exist elsewhere and add to the high diversity of arc and back-arc hydrothermal systems. As volcanic activity might be waning and waxing transient changes in fluid composition can be expected within months or years. If the fluid circulation pathways within the plumbing system become more stable over time an increase in salinity and Li/Cl, decrease in Fe and REY, development of a more pronounced HREE enrichment and Eu anomaly, might be expected as water/rock ratios decrease and an equilibrium is established between circulating fluid and host rock.

6. Acknowledgements

We thank Captain D. Korte and his crew for their skilled support of the scientific work onboard RV *Sonne* and we acknowledge the excellent cooperation with the ROV *Kiel6000* crew. We also thank Charlotte Kleint for her support during fluid sampling, and sample treatment on board. Ulrike Westernströer, Jule Mawick and Daniela Meissner are thanked for their help with geochemical analyses in the laboratories at Kiel University and Jacobs University, Bremen. We are grateful to Tim McConachy of Neptune Minerals, Inc. giving us access to δ^3He samples from a 2010 survey above the Nifonea hydrothermal field. Adalbert Wilhelm from the Jacobs University Bremen is highly acknowledged for his help with statistical evaluation. We thank Nico Augustin (GEOMAR) for providing the bathymetric map. The critical comments of three anonymous reviewers strongly improved the quality of the first version of this manuscript. The funding of the project 03G 0229 by the BMBF German Federal Ministry of Education and Research is gratefully acknowledged.

References

Allen D. E. and Seyfried W. E. (2005) REE controls in ultramafic hosted MOR hydrothermal systems: An experimental study at elevated temperature and pressure. *Geochim. Cosmochim. Acta* **69**, 675–683.

Anderson M. O., Hannington M. D., Haase K., Schwarz-Schampera U., Augustin N.,

McConachy T. F. and Allen K. (2016) Tectonic focusing of voluminous basaltic eruptions in magma-deficient backarc rifts. *Earth Planet. Sci. Lett.* **440**, 43–55.

Bach W. and Irber W. (1998) Rare earth element mobility in the oceanic lower sheeted dyke complex: evidence from geochemical data and leaching experiments. *Chem. Geol.* **151**, 309–326.

Bau M. (1991) Rare-earth element mobility during hydrothermal and metamorphic fluid-rock interaction and the significance of the oxidation state of europium. *Chem. Geol.* **93**, 219–230.

Bau M. and Dulski P. (1999) Comparing yttrium and rare earths in hydrothermal fluids from the Mid-Atlantic Ridge: implications for Y and REE behaviour during near-vent mixing and for the Y/Ho ratio of Proterozoic seawater. *Chem. Geol.* **155**, 77–90.

Bau M., Usui A., Pracejus B., Mita N., Kanai Y., Irber W. and Dulski P. (1998) Geochemistry of low-temperature water–rock interaction: evidence from natural waters, andesite, and iron-oxyhydroxide precipitates at Nishiki-numa iron-spring, Hokkaido, Japan. *Chem. Geol.* **151**, 293–307.

Bennett S. A., Achterberg E. P., Connelly D. P., Statham P. J., Fones G. R. and German C. R. (2008) The distribution and stabilisation of dissolved Fe in deep-sea hydrothermal plumes. *Earth Planet. Sci. Lett.* **270**, 157–167.

Beermann O., Garbe-Schönberg D., Bach W. and Holzheid A. (2017) Time-resolved interaction of seawater with gabbro: An experimental study of rare-earth element behavior up to 475°C, 100MPa. *Geochim. Cosmochim. Acta* **197**, 167–192.

Berndt M. E. and Seyfried W. E. (1990) Boron, bromine, and other trace elements as clues to the fate of chlorine in mid-ocean ridge vent fluids. *Geochim. Cosmochim. Acta* **54**, 2235–2245.

Breuer C. and Pichler T. (2013) Arsenic in marine hydrothermal fluids. *Chem. Geol.* **348**, 2–14.

Butterfield D. A., Jonasson I. R., Massoth G. J., Feely R. A., Roe K. K., Embley R. E., Holden J. F., McDuff R. E., Lilley M. D. and Delaney J. R. (1997) Seafloor eruptions and evolution of hydrothermal fluid chemistry. *Philos. Trans. R. Soc. London A Math. Phys. Eng. Sci.* **355**, 369–386.

Charlou J. L., Donval J. P., Jean-Baptiste P., Dapoigny A. and Rona P. A. (1996) Gases and helium isotopes in high temperature solutions sampled before and after ODP Leg 158 drilling at TAG Hydrothermal Field (26°N, MAR). *Geophys. Res. Lett.* **23**, 3491–3494.

Cole C. S., James R. H., Connelly D. P. and Hathorne E. C. (2014) Rare earth elements as indicators of hydrothermal processes within the East Scotia subduction zone system. *Geochim. Cosmochim. Acta* **140**, 20–38.

Craddock P. R. (2009) Geochemical tracers of processes affecting the formation of seafloor hydrothermal fluids and deposits in the Manus back-arc basin. Massachusetts Institute of Technology and Woods Hole Oceanographic Institution, PhD thesis.

Craddock P. R., Bach W., Seewald J. S., Rouxel O. J., Reeves E. and Tivey M. K. (2010) Rare earth element abundances in hydrothermal fluids from the Manus Basin, Papua New Guinea: Indicators of sub-seafloor hydrothermal processes in back-arc basins. *Geochim. Cosmochim. Acta* **74**, 5494–5513.

Douville E., Charlou J. L., Oelkers E. H., Bienvenu P., Jove Colon C. F., Donval J. P., Fouquet Y., Prieur D. and Appriou P. (2002) The rainbow vent fluids (36°14′N, MAR): the influence of ultramafic rocks and phase separation on trace metal content in Mid-

963 Atlantic Ridge hydrothermal fluids. *Chem. Geol.* **184**, 37–48.

964 Douville E., Charlou J.-L., Donval J.-P., Hureau D. and Appriou P. (1999) Le comportement
965 de l'arsenic (As) et de l'antimoine (Sb) dans les fluides provenant de différents systèmes
966 hydrothermaux océaniques. *Comptes Rendus l'Académie des Sci. - Ser. IIA - Earth*
967 *Planet. Sci.* **328**, 97–104.

968 Driesner T. (2007) The system H2O–NaCl. Part II: Correlations for molar volume, enthalpy,
969 and isobaric heat capacity from 0 to 1000°C, 1 to 5000bar, and 0 to 1 XNaCl. *Geochim.*
970 *Cosmochim. Acta* **71**, 4902–4919.

971 Driesner T. and Heinrich C. A. (2007) The system H2O–NaCl. Part I: Correlation formulae
972 for phase relations in temperature–pressure–composition space from 0 to 1000°C, 0 to
973 5000bar, and 0 to 1 XNaCl. *Geochim. Cosmochim. Acta* **71**, 4880–4901.

974 Escoube R., Rouxel O. J., Edwards K., Glazer B. and Donard O. F. X. (2015) Coupled Ge/Si
975 and Ge isotope ratios as geochemical tracers of seafloor hydrothermal systems: Case
976 studies at Loihi Seamount and East Pacific Rise 9°50′N. *Geochim. Cosmochim. Acta*
977 **167**, 93–112.

978 Fontaine F. J., Wilcock W. S. D., Foustoukos D. E. and Butterfield D. A. (2009) A Si-Cl
979 geothermobarometer for the reaction zone of high-temperature, basaltic-hosted mid-
980 ocean ridge hydrothermal systems. *Geochemistry, Geophys. Geosystems* **10**, Q05009.

981 Fornari D. F., Von Damm K. L., Bryce J. G., Cowen J. P., Ferrini V., Fundis A., Lilley M. D.,
982 Luther III G. W., Mullineaux L. S., Perfit M. R., Meana-Prado M. F., Rubin K. H.,
983 Seyfried Jr. W. E., Shank T. M., Tolstoy M. and White S. M. (2012) The East Pacific
984 Rise Between 9°N and 10°N: Twenty-Five Years of Integrated, Multidisciplinary
985 Oceanic Spreading Center Studies. *Oceanography* **25**.

986 Fourre E., Jean-Baptiste P., Charlou J.-L., Donval J.P., and Ishibashi J.I. (2006) Helium
987 isotopic composition of hydrothermal fluids from the Manus back-arc Basin, Papua New
988 Guinea. *Geochem. J.* **40**, 245–252.

989 Foustoukos D. I. and Seyfried W. E. (2007a) Quartz solubility in the two-phase and critical
990 region of the NaCl–KCl–H2O system: Implications for submarine hydrothermal vent
991 systems at 9°50′N East Pacific Rise. *Geochim. Cosmochim. Acta* **71**, 186–201.

992 Foustoukos D. I. and Seyfried W. E. (2007b) Trace element partitioning between vapor, brine
993 and halite under extreme phase separation conditions. *Geochim. Cosmochim. Acta* **71**,
994 2056–2071.

995 Gamo T., Okamura K., Charlou J.-L., Urabe T., Auzende J.-M., Ishibashi J., Shitashima K.,
996 Chiba H. and Cruise S. S. P. of the M. (1997) Acidic and sulfate-rich hydrothermal fluids
997 from the Manus back-arc basin, Papua New Guinea. *Geol.* **25** , 139–142.

998 Garbe-Schönberg D., Koschinsky A., Ratmeyer V., Jähmlich H. and Westernströer U. (2006)
999 KIPS—A new multiport valve-based all-Teflon fluid sampling system for ROVs. In
1000 *Geophys. Res. Abstr. 8* p. 07032.

1001 Giese R. and Bau M. (1994) Trace element accessibility in mid-ocean ridge and ocean island
1002 basalt: an experimental approach. *Min. Mag.* **58A**, 329–330.

1003 Haase K. M., Petersen S., Koschinsky A., Seifert R., Devey C. W., Keir R., Lackschewitz K.
1004 S., Melchert B., Perner M., Schmale O., Süling J., Dubilier N., Zielinski F., Fretzdorff S.,
1005 Garbe-Schönberg D., Westernströer U., German C. R., Shank T. M., Yoerger D., Giere
1006 O., Kuever J., Marbler H., Mawick J., Mertens C., Stöber U., Walter M., Ostertag-
1007 Henning C., Paulick H., Peters M., Strauss H., Sander S., Stecher J., Warmuth M. and
1008 Weber S. (2007) Young volcanism and related hydrothermal activity at 5°S on the slow-

spreading southern Mid-Atlantic Ridge. *Geochemistry, Geophys. Geosystems* **8**.

Haase K. M. and Scientists S.-229 S. (2013) Volcanism, hydrothermal activity and vent biology in the Coriolis Troughs, New Hebrides Island Arc.,Cruise Report COVOLVE, SO229.

Hannington M. D., Jonasson I. R., Herzig P. M. and Petersen S. (1995) Physical and Chemical Processes of Seafloor Mineralization at Mid-Ocean Ridges. In *Seafloor Hydrothermal Systems: Physical, Chemical, Biological, and Geological Interactions* American Geophysical Union. pp. 115–157.

Heinrich C. A., Günther D., Audétat A., Ulrich T. and Frischknecht R. (1999) Metal fractionation between magmatic brine and vapor, determined by microanalysis of fluid inclusions. *Geol.* **27** , 755–758.

Herzig P. M., Hannington M. D. and Arribas Jr. A. (1998) Sulfur isotopic composition of hydrothermal precipitates from the Lau back-arc: implications for magmatic contributions to seafloor hydrothermal systems. *Miner. Depos.* **33**, 226–237.

Ibrahim A. K., Pontoise B., Latham G., Larue M., Chen T., Isacks B., Recy J. and Louat R. (1980) Structure of the New Hebrides Arc-Trench System. *J. Geophys. Res. Solid Earth* **85**, 253–266.

Iizasa K., Kawasaki K., Maeda K., Matsumoto T., Saito N. and Hirai K. (1998) Hydrothermal sulfide-bearing Fe-Si oxyhydroxide deposits from the Coriolis Troughs, Vanuatu backarc, southwestern Pacific. *Mar. Geol.* **145**, 1–21.

Ishibashi J., Tsunogai U., Toki T., Ebina N., Gamo T., Sano Y., Masuda H. and Chiba H. (2015) Chemical composition of hydrothermal fluids in the central and southern Mariana Trough backarc basin. *Deep Sea Res. Part II Top. Stud. Oceanogr.* **121**, 126–136.

Ishibashi J.-I., Wakita H., Nojiri Y., Grimaud D., Jean-Baptiste P., Gamo T., Auzende J.-M. and Urabe T. (1994) Helium and carbon geochemistry of hydrothermal fluids from the North Fiji Basin spreading ridge (southwest Pacific). *Earth Planet. Sci. Lett.* **128**, 183–197.

James R. H., Green D. R. H., Stock M. J., Alker B. J., Banerjee N. R., Cole C., German C. R., Huvenne V. A. I., Powell A. M. and Connelly D. P. (2014) Composition of hydrothermal fluids and mineralogy of associated chimney material on the East Scotia Ridge back-arc spreading centre. *Geochim. Cosmochim. Acta* **139**, 47–71.

James R. H., Elderfield H. and Palmer M. R. (1995) The chemistry of hydrothermal fluids from the Broken Spur site, 29°N Mid-Atlantic ridge. *Geochim. Cosmochim. Acta* **59**, 651–659.

Jean-Baptiste P., Allard P., Fourré E., Bani P., Calabrese S., Aiuppa A., Gauthier P. J., Parello F., Pelletier B. and Garaebiti E. (2015) Spatial distribution of helium isotopes in volcanic gases and thermal waters along the Vanuatu (New Hebrides) volcanic arc. *J. Volcanol. Geotherm. Res* **332**, 20-29..

Lima S. M., Haase K. M., Beier C., Regelous M., Brandl P. A., Hauff F. and Krumm S. Magmatic evolution and source variations at the Nifonea Ridge (New Hebrides Island Arc). (in revision) *J. Petrol.*

Lupton J. E., Arculus R. J., Greene R. R., Evans L. J. and Goddard C. I. (2009) Helium isotope variations in seafloor basalts from the Northwest Lau Backarc Basin: Mapping the influence of the Samoan hotspot. *Geophys. Res. Lett.* **36**, L17313.

Lupton J. E., Arculus R. J., Jenner F. E., Evans L. and Greene R. (2012) Helium Isotope Variations in the Northern Lau and North Fiji Basins. *AGU Fall Meet. Abstr.*, V23B–

2820.

Lupton J., Rubin K. H., Arculus R., Lilley M., Butterfield D., Resing J., Baker E. and Embley R. (2015) Helium isotope, C/ 3 He, and Ba-Nb-Ti signatures in the northern Lau Basin: Distinguishing arc, back-arc, and hotspot affinities. *Geochemistry, Geophys. Geosystems* **16**, 1133–1155.

McConachy T. F., Arculus R. J., Yeats C. J., Binns R. A., Barriga F. J. A. S., McInnes B. I. A., Sestak S., Sharpe R., Rakau B. and Tevi T. (2005) New hydrothermal activity and alkalic volcanism in the backarc Coriolis Troughs, Vanuatu. *Geol.* **33** , 61–64.

Metz S. and Trefry J. H. (2000) Chemical and mineralogical influences on concentrations of trace metals in hydrothermal fluids. *Geochim. Cosmochim. Acta* **64**, 2267–2279.

Monjaret M.J., Bellon H., Maillet P. (1991) Magmatism of the troughs behind the New Hebrides island arc (RV Jean Charcot SEAPSO 2 cruise): K-Ar geochronology and petrology. *Journal of Volcanology and Geothermal Research* **46**, 265-280.

Mortlock R. A., Froelich P. N., Feely R. A., Massoth G. J., Butterfield D. A. and Lupton J. E. (1993) Silica and germanium in Pacific Ocean hydrothermal vents and plumes. *Earth Planet. Sci. Lett.* **119**, 365–378.

Mottl M. J. and Holland H. D. (1978) Chemical exchange during hydrothermal alteration of basalt by seawater—I. Experimental results for major and minor components of seawater. *Geochim. Cosmochim. Acta* **42**, 1103–1115.

Mottl M. J., Seewald J. S., Wheat C. G., Tivey M. K., Michael P. J., Proskurowski G., McCollom T. M., Reeves E., Sharkey J., You C.-F., Chan L.-H. and Pichler T. (2011) Chemistry of hot springs along the Eastern Lau Spreading Center. *Geochim. Cosmochim. Acta* **75**, 1013–1038.

Ogawa Y., Shikazono N., Ishiyama D., Sato H. and Mizuta T. (2005) An experimental study on felsic rock--artificial seawater interaction: implications for hydrothermal alteration and sulfate formation in the Kuroko mining area of Japan. *Miner. Depos.* **39**, 813–821.

Peate D. W., Pearce J. A., Hawkesworth C. J., Colley H., Edwards C. M. H. and Hirose K. (1997) Geochemical Variations in Vanuatu Arc Lavas: the Role of Subducted Material and a Variable Mantle Wedge Composition. *J. Petrol.* **38** , 1331–1358.

Pester N. J., Ding K. and Seyfried W. E. (2014) Magmatic eruptions and iron volatility in deep-sea hydrothermal fluids. *Geol.* **42**, 255-258.

Pester N. J., Ding K. and Seyfried W. E. (2015) Vapor–liquid partitioning of alkaline earth and transition metals in NaCl-dominated hydrothermal fluids: An experimental study from 360 to 465°C, near-critical to halite saturated conditions. *Geochim. Cosmochim. Acta* **168**, 111–132.

Pester N. J., Rough M., Ding K. and Seyfried W. E. (2011) A new Fe/Mn geothermometer for hydrothermal systems: Implications for high-salinity fluids at 13°N on the East Pacific Rise. *Geochim. Cosmochim. Acta* **75**, 7881–7892.

Pokrovski G. S., Borisova A. Y. and Harrichoury J.-C. (2008) The effect of sulfur on vapor–liquid fractionation of metals in hydrothermal systems. *Earth Planet. Sci. Lett.* **266**, 345–362.

Pokrovski G. S., Roux J. and Harrichoury J.-C. (2005) Fluid density control on vapor-liquid partitioning of metals in hydrothermal systems. *Geol.* **33** , 657–660.

Price R. C., Maillet P. and Johnson D. P. (1993) Interpretation of GLORIA side-scan sonar imagery for the Coriolis Troughs of the New Hebrides backarc. *Geo-Marine Lett.* **13**,

71–81.

Reeves E. P., Seewald J. S., Saccocia P., Bach W., Craddock P. R., Shanks W. C., Sylva S. P., Walsh E., Pichler T. and Rosner M. (2011) Geochemistry of hydrothermal fluids from the PACMANUS, Northeast Pual and Vienna Woods hydrothermal fields, Manus Basin, Papua New Guinea. *Geochim. Cosmochim. Acta* **75**, 1088–1123.

Resing J. A., Lebon G., Baker E. T., Lupton J. E., Embley R. W., Massoth G. J., Chadwick W. W. and de Ronde C. E. J. (2007) Venting of Acid-Sulfate Fluids in a High-Sulfidation Setting at NW Rota-1 Submarine Volcano on the Mariana Arc. *Econ. Geol.* **102** , 1047–1061.

Resing J. A., Sedwick P. N., German C. R., Jenkins W. J., Moffett J. W., Sohst B. M. and Tagliabue A. (2015) Basin-scale transport of hydrothermal dissolved metals across the South Pacific Ocean. *Nature* **523**, 200–203.

de Ronde C. E. J., Hannington M. D., Stoffers P., Wright I. C., Ditchburn R. G., Reyes A. G., Baker E. T., Massoth G. J., Lupton J. E., Walker S. L., Greene R. R., Soong C. W. R., Ishibashi J., Lebon G. T., Bray C. J. and Resing J. A. (2005) Evolution of a Submarine Magmatic-Hydrothermal System: Brothers Volcano, Southern Kermadec Arc, New Zealand. *Econ. Geol.* **100** , 1097–1133.

de Ronde C. E. J., Massoth G. J., Butterfield D. A., Christenson B. W., Ishibashi J., Ditchburn R. G., Hannington M. D., Brathwaite R. L., Lupton J. E., Kamenetsky V. S., Graham I. J., Zellmer G. F., Dziak R. P., Embley R. W., Dekov V. M., Munnik F., Lahr J., Evans L. J. and Takai K. (2011) Submarine hydrothermal activity and gold-rich mineralization at Brothers Volcano, Kermadec Arc, New Zealand. *Miner. Depos.* **46**, 541–584.

Sander S. G. and Koschinsky A. (2011) Metal flux from hydrothermal vents increased by organic complexation. *Nat. Geosci* **4**, 145–150.

Schmidt K., Garbe-Schönberg D., Koschinsky A., Strauss H., Jost C. L., Klevenz V. and Königer P. (2011) Fluid elemental and stable isotope composition of the Nibelungen hydrothermal field (8°18′S, Mid-Atlantic Ridge): Constraints on fluid–rock interaction in heterogeneous lithosphere. *Chem. Geol.* **280**, 1–18.

Schmidt K., Koschinsky A., Garbe-Schönberg D., Decarvallo L. and Seifert R. (2007) Geochemistry of hydrothermal fluids from the ultramafic-hosted Logatchev hydrothermal field, 15°N on the Mid-Atlantic Ridge: Temporal and spatial investigation. *Chem. Geol.* **242**, 1–21.

Seewald J. S., Reeves E. P., Bach W., Saccocia P. J., Craddock P. R., Shanks W. C., Sylva S. P., Pichler T., Rosner M. and Walsh E. (2015) Submarine venting of magmatic volatiles in the Eastern Manus Basin, Papua New Guinea. *Geochim. Cosmochim. Acta* **163**, 178–199.

Seyfried Jr. W. E., Ding K., Berndt M. E. and Chen X. (1999) Experimental and theoretical controls on the composition of mid-ocean ridge hydrothermal fluids. In *Volcanic associated massive sulfide deposits: Processes and examples in modern and ancient settings* (eds. T. Barrie and M. D. Hannington). pp. 181–200.

Seyfried W. E. and Ding K. (1995) Phase Equilibria in Subseafloor Hydrothermal Systems: a Review of the Role of Redox, Temperature, Ph and Dissolved Cl on the Chemistry of Hot Spring Fluids at Mid-Ocean Ridges. In *Seafloor Hydrothermal Systems: Physical, Chemical, Biological, and Geological Interactions* American Geophysical Union. pp. 248–272.

Seyfried W. E., Seewald J. S., Berndt M. E., Ding K. and Foustoukos D. I. (2003) Chemistry

of hydrothermal vent fluids from the Main Endeavour Field, northern Juan de Fuca Ridge: Geochemical controls in the aftermath of June 1999 seismic events. *J. Geophys. Res. Solid Earth* **108**, 2429.

Shanks W. C. (2001) Stable Isotopes in Seafloor Hydrothermal Systems: Vent fluids, hydrothermal deposits, hydrothermal alteration, and microbial processes. *Rev. Mineral. Geochemistry* **43** , 469–525.

Shibata S.-N., Tanaka T. and Yamamoto K. (2006) Crystal structure control of the dissolution of rare earth elements in water-mineral interactions. *Geochem. J.* **40**, 437–446.

Takai K., Nunoura T., Ishibashi J., Lupton J., Suzuki R., Hamasaki H., Ueno Y., Kawagucci S., Gamo T., Suzuki Y., Hirayama H. and Horikoshi K. (2008) Variability in the microbial communities and hydrothermal fluid chemistry at the newly discovered Mariner hydrothermal field, southern Lau Basin. *J. Geophys. Res. Biogeosciences* **113**,

Tertre E., Hofmann A. and Berger G. (2008) Rare earth element sorption by basaltic rock: Experimental data and modeling results using the "Generalised Composite approach." *Geochim. Cosmochim. Acta* **72**, 1043–1056.

Trefry J. H., Butterfield D. B., Metz S., Massoth G. J., Trocine R. P. and Feely R. A. (1994) Trace metals in hydrothermal solutions from Cleft segment on the southern Juan de Fuca Ridge. *J. Geophys. Res. Solid Earth* **99**, 4925–4935.

Von Damm K. L. (2000) Chemistry of hydrothermal vent fluids from 9°–10°N, East Pacific Rise: "Time zero," the immediate posteruptive period. *J. Geophys. Res. Solid Earth* **105**, 11203–11222.

Von Damm K. L. (2004) Evolution of the Hydrothermal System at East Pacific Rise 9°50´N: Geochemical Evidence for Changes in The Upper Oceanic Crust. In *Mid-Ocean Ridges* American Geophysical Union. pp. 285–304.

Von Damm K. L. (1990) Seafloor Hydrothermal Activity: Black Smoker Chemistry and Chimneys. *Annu. Rev. Earth Planet. Sci.* **18**, 173–204.

Von Damm K. L., Bischoff J. L. and Rosenbauer R. J. (1991) Quartz solubility in hydrothermal seawater; an experimental study and equation describing quartz solubility for up to 0.5 M NaCl solutions. *Am. J. Sci.* **291** , 977–1007.

Von Damm K. L., Edmond J. M., Measures C. I. and Grant B. (1985) Chemistry of submarine hydrothermal solutions at Guaymas Basin, Gulf of California. *Geochim. Cosmochim. Acta* **49**, 2221–2237.

Von Damm K. L., Oosting S. E., Kozlowski R., Buttermore L. G., Colodner D. C., Edmonds H. N., Edmond J. M. and Grebmeier J. M. (1995) Evolution of East Pacific Rise hydrothermal vent fluids following a volcanic eruption. *Nature* **375**, 47–50.

Wheat C. G. and McManus J. (2008) Germanium in mid-ocean ridge flank hydrothermal fluids. *Geochemistry, Geophys. Geosystems* **9**.

Williams-Jones A. E. and Heinrich C. A. (2005) 100th Anniversary Special Paper: Vapor Transport of Metals and the Formation of Magmatic-Hydrothermal Ore Deposits. *Econ. Geol.* **100** , 1287–1312.

Young C. and Lupton J. E. (1983) An ultratight fluid sampling system using cold-welded copper tubing. *Eos Trans. AGU* **64**, 735.

Yücel M. and Luther G. W. (2013) Temporal trends in vent fluid iron and sulfide chemistry following the 2005/2006 eruption at East Pacific Rise, 9°50′N. *Geochemistry, Geophys. Geosystems* **14**, 759–765.

1191 Zeng Z., Niedermann S., Chen S., Wang X. and Li Z. (2015) Noble gases in sulfide deposits
1192 of modern deep-sea hydrothermal systems: Implications for heat fluxes and
1193 hydrothermal fluid processes. *Chem. Geol.* **409**, 1–11.

1194

1195

Table 1

Table 1: Fluid sampling stations in the Nifonea vent field

Vent site	Water Depth [m]	Latitude/Longitude	Fluid samples	T [°C]	Remarks
NIF 1	1862	18°7.758'S / 169°31.039'E	27 ROV-14 A,B,C	>>250	2.5–3 m high black smoker, fluid samples taken before collapse of the chimney
			66 ROV-1	107	7 days after first sampling, re-grown black smoker chimney (20–30 cm tall)
NIF-2	1873	18°7.734'S / 169°31.106'E	60 ROV-1 B,C,D	345	Clear fluid, 1-2 cm tall juvenile chimney structures
NIF-3	1862	18°7.753'S / 169°31.040'E	66 ROV-6	165	Black smoker, fluid sample taken from open sulfide chimney,
NIF-4	1862	18°7.758'S / 169°31.043'E	77 ROV-6	368	30–40 cm tall black smoker, same chimney cluster as NIF-1
NIF-5	1862	18°7.742'S / 169°31.073'E	77 ROV-10,11	368	Black smoker chimney, <1 m tall, several orifices
NIF-7	1862	18°7.758'S / 169°31.039'E	66 ROV-3,5	132	Same chimney complex with NIF-1

Table 2a

Table 2a: Measured major, minor, and trace element concentrations in Nifonea vent fluids, n.a.: not analyzed

Vent Site	Sample ID	T	pH	SO_4	H_2S	EM	Mg	Cl	Br	B	Si	Ge	Al	Na	K	Li	Rb	Cs	Ca	Sr	Ba
		℃		*mM*	*µM*	%	*mM*	*mM*	*mM*	*µM*	*mM*	*nM*	*µM*	*mM*	*mM*	*µM*	*µM*	*nM*	*mM*	*µM*	*µM*
ambient SW	**56 CTD 1900**	4		28	0		52.8	545	0.806	419	0.102	0.399	0.1	474	10.5	26.5	1.49	1.9	10.4	90.9	0.107
NIF-1	**27 ROV 14 KIPS A**	(>250)				23	41.5	448	0.682	594	1.24	n.a.	n.a.	379	8.29	21.9	n.a.	n.a.	11.2	73.5	n.a.
	27 ROV 14 KIPS B	(>250)	3.3			77	12.3	173	0.279	902	3.5	13.2	1.15	141	3.11	9.95	0.527	1.96	10.1	32.7	8.46
	27 ROV 14 KIPS C	(>250)		8		72	15.1	193	0.301	843	3.14	13.1	0.934	163	3.58	11.1	0.595	1.91	9.35	35.6	7.5
	66 ROV 1 KIPS B	107	4.4	12	7800	49	27.6	311	0.47	715	2.31	n.a.	n.a.	267	5.79	16.2	0.938	2.4	9.87	53.6	n.a.
NIF-2	**60 ROV 1 KIPS B**	345	4.7	19	7800	53	25.4	296	0.456	774	4.3	20.3	21.7	257	5.75	16.7	0.958	2.39	9.55	50.9	3.3
	60 ROV 1 KIPS C	345		19	3400	21	42.5	462	0.695	587	2.52	12.4	5.65	394	8.68	23.3	1.31	2.33	11.4	76.5	2
	60 ROV 1 KIPS D	345				22	42.2	456	0.7	606	2.66	n.a.	n.a.	395	8.74	25.2	n.a.	n.a.	11.7	76.8	n.a.
NIF-3	**66 ROV 6 KIPS D**	165		18	1600	20	43.3	458	0.687	549	1.62	5.73	0.267	391	8.51	22.3	1.26	1.69	9.73	73.5	1.55
NIF-4	**77 ROV 6 KIPS A**	368	2.9	8	4700	73	14.9	340	0.505	1140	4.09	23.4	3.16	255	6.31	29.8	1.16	7.78	28.2	64.1	4.34
NIF-5	**77 ROV 10 KIPS B**	368	3.4	4	6200	93	3.82	62.7	0.113	1480	4.94	25.5	2.02	53.4	1.11	3.93	0.191	0.587	5.67	17.4	3.16
NIF-7	**66 ROV 3 KIPS C**	132		19	1600	20	43.2	484	0.738	563	1.02	5.41	0.65	409	9.11	25.6	1.4	1.72	13.8	79.5	6.28
	66 ROV 5 NISKIN					4	51.7	545	0.809	438	0.228	1.1	0.274	462	10.1	25.6	1.43	2.05	11.1	86.4	1.03

Table 2a continued: Measured major, minor, and trace element concentrations in Nifonea vent fluids, n.a.: not analyzed

Vent Site	Sample ID	Fe	Mn	Co	Ni	Cu	Zn	Cd	Ag	Ga	In	Sn	Pb	Tl	As	Se	Sb	Mo	W	U
		µM	*µM*	*nM*	*nM*	*µM*	*µM*	*nM*	*nM*	*nM*	*nM*	*nM*	*nM*	*nM*	*nM*	*nM*	*nM*	*nM*	*nM*	*nM*
ambient SW	**56 CTD 1900**	0.005	n.a.	n.a.	0.92	0.006	0.096	0.783	n.a.	0.0287	n.a.	n.a.	1.07	0.044	23.7	0.279	1.62	139	0.315	12.9
	27 ROV 14 KIPS B	892	406	12.3	0.937	2.41	36.6	38.9	2.86	5.88	3.09	1.46	280	31.6	7480	105	13.3	45.4	1.41	3.13
	27 ROV 14 KIPS C	881	412	3.68	26	1.08	30.5	23.9	1.38	2.95	1.56	0.211	276	25.2	7420	49.3	7.97	45.9	2.53	3.77
	66 ROV 1 KIPS B	n.a.	n.a.	n.a.	n.a.	n.a.	n.a.	n.a.	n.a.	n.a.	n.a.	n.a.	n.a.	n.a.	n.a.	n.a.	n.a.	n.a.	n.a.	n.a.
NIF-2	**60 ROV 1 KIPS B**	89.8	171	4.46	39	1.06	19.5	40.3	1.78	4.46	1.19	0.842	143	9	7820	17.2	14.5	77.4	1.64	6.11
	60 ROV 1 KIPS C	46.4	90.5	<	15.8	0.668	13	30	0.732	2.68	0.923	0.505	71.8	3.38	3140	-	7.41	91	1.2	10.2
	60 ROV 1 KIPS D	n.a.	n.a.	n.a.	n.a.	n.a.	n.a.	n.a.	n.a.	n.a.	n.a.	n.a.	n.a.	n.a.	n.a.	n.a.	n.a.	n.a.	n.a.	
NIF-3	**66 ROV 6 KIPS D**	136	52.5	<	5.11	0.003	4.83	8.74	<	1.15	0.34	<	43.1	3.06	193	< 0.1	0.468	29	0.925	10.4
NIF-4	**77 ROV 6 KIPS A**	5300	1510	273	54.8	23.2	166	370	27	50.4	19.2	5.7	1590	93.3	15400	317	63.9	135	2.52	5.72
NIF-5	**77 ROV 10 KIPS B**	628	92.8	67.3	11.4	8.97	63.8	123	4.8	15.2	7.85	2.03	473	25	19200	154	30.1	30.5	0.767	1.24
NIF-7	**66 ROV 3 KIPS C**	864	271	0.611	<	1.19	14.9	25	1.19	2.95	1.2	0.278	144	8.56	1990	2.53	4.63	54.6	1.01	10.7
	66 ROV 5 NISKIN	131	40.8	<	<	0.648	5.75	10.6	0.621	1.35	0.462	0.581	65.4	3.89	675	2.57	3.52	121	0.87	12.1

Table 2b

Table 2b: Calculated endmember composition of Nifonea vent fluids, EM; endmember; R^2: correlation coefficient; n.a.: not analyzed

Vent Site		SO_4	H_2S	Cl	Br	B	Si	Ge	Al	Na	K	Li	Rb	Cs	Ca	Sr	Ba
		mM	*µM*	*mM*	*mM*	*µM*	*mM*	*nM*	*µM*	*mM*	*mM*	*µM*	*µM*	*nM*	*mM*	*µM*	*µM*
NIF-1	**endmember**	**-1.37**	**10600**	**55.5**	**0.107**	**1030**	**4.47**	**17.6**	**1.41**	**39.5**	**0.827**	**4.92**	**0.246**	**2.06**	**9.4**	**14.2**	**10.8**
	R^2	*0.99*	*-0.86*	*1.00*	*1.00*	*-0.99*	*-1.00*	*-1.00*	*-0.99*	*1.00*	*1.00*	*1.00*	*1.00*	*-0.05*	*0.66*	*1.00*	*-1.00*
	uncertainty of regression	2.11	2930	**11.7**	0.0167	39.7	0.161	0.657	0.0518	9.29	0.211	0.586	0.0318	0.293	0.594	1.96	0.397
NIF-2	**endmember**	**10.1**	**15100**	**66.5**	**0.136**	**1110**	**8.33**	**39.2**	**41.6**	**56.4**	**1.35**	**7.88**	**0.467**	**2.87**	**9**	**14**	**6.33**
	R^2	*0.79*	*-1.00*	*1.00*	*1.00*	*-0.99*	*-0.96*	*-0.97*	*-0.99*	*1.00*	*1.00*	*0.96*	*1.00*	*-0.85*	*0.50*	*1.00*	*-0.97*
	uncertainty of regression	4.54	1040	**34.6**	0.052	79.2	0.62	3.65	2.95	31.5	0.679	1.77	0.0992	0.247	1.04	5.76	0.56
	endmember[#]	**10.7**	**15000**	**65.2**	**0.132**	**1100**	**8.19**	**38.7**	**41.7**	**55.8**	**1.35**	**7.62**	**0.465**	**2.84**	**8.76**	**13.8**	**6.26**
	uncertainty of regression	2.57	1220	52.9	0.0753	88.7	0.64	2.91	3.68	44.2	0.986	2.69	0.138	0.257	1.11	8.61	0.493
NIF-4	**endmember**	**0.137**	**6550**	**259**	**0.387**	**1420**	**5.66**	**32.4**	**4.4**	**169**	**4.66**	**31.1**	**1.03**	**10.1**	**35.2**	**53.6**	**6**
	uncertainty of regression	0.81	372	**24.5**	0.0356	77.4	0.295	1.71	0.236	18.8	0.454	2.04	0.0817	0.569	2.08	4.48	0.329
NIF-5	**endmember**	**2.13**	**6680**	**25.1**	**0.059**	**1560**	**5.32**	**27.5**	**2.18**	**20.6**	**0.378**	**2.17**	**0.0897**	**0.485**	**5.3**	**11.7**	**3.4**
	uncertainty of regression	0.242	353	**3.93**	0.0066	75.4	0.259	1.35	0.109	3.37	0.0706	0.229	0.0118	0.0327	0.316	0.969	0.175

[#] based only on sample 60 ROV-1 KIPS B

Table 2b continued: Calculated endmember composition of Nifonea vent fluids, EM; endmember; R^2: correlation coefficient; n.a.: not analyzed

Vent Site		Fe	Mn	Co	Ni	Cu	Zn	Cd	Ag	Ga	In	Sn	Pb	Tl	As	Se	Sb	Mo	W	U
		µM	*µM*	*nM*	*nM*	*µM*	*µM*	*nM*	*nM*	*nM*	*nM*	*nM*	*nM*	*nM*	*nM*	*nM*	*nM*	*nM*	*nM*	*nM*
NIF-1	**endmember**	**1200**	**551**	**11.1**	**16.9**	**2.4**	**45.4**	**42.6**	**2.91**	**6.05**	**3.19**	**1.17**	**374**	**38.5**	**10000**	**106**	**14**	**13.2**	**2.5**	**0.14**
	R^2	*-1.00*	*-1.00*	*-0.77*	*-0.45*	*-0.87*	*-1.00*	*-0.94*	*-0.89*	*-0.89*	*-0.90*	*-0.66*	*-1.00*	*-0.99*	*-1.00*	*-0.88*	*-0.92*	*1.00*	*-0.83*	*1.00*
	uncertainty of regression	44.9	24.9	5.68	18.3	0.851	2.61	9.04	0.937	1.85	0.962	0.839	14.2	3.08	380	35.4	3.31	4.37	0.874	0.221
NIF-2	**endmember**	**174**	**332**	**8.59**	**74.4**	**2.06**	**38**	**78.3**	**3.44**	**8.66**	**2.34**	**1.64**	**276**	**17.3**	**15100**	**32.9**	**26.5**	**17.9**	**2.91**	**-0.198**
	R^2	*-0.99*	*-0.98*	*-1.00*	*-1.00*	*-0.96*	*-0.95*	*-0.92*	*-1.00*	*-0.97*	*-0.90*	*-0.97*	*-0.99*	*-1.00*	*-1.00*	*-1.00*	*-1.00*	*0.90*	*-0.94*	*1.00*
	uncertainty of regression	12.3	22.3	0.584	5.03	0.215	4.53	11.6	0.233	0.797	0.384	0.152	19.3	1.19	1000	2.31	1.76	20.1	0.313	0.844
	endmember[#]	**173**	**374**	**9.76**	**74.3**	**2.04**	**37.5**	**76.9**	**3.89**	**8.57**	**2.6**	**1.84**	**275**	**17.3**	**15000**	**32.9**	**26.4**	**20.3**	**2.87**	**-0.184**
	uncertainty of regression	13.9	25.6	0.738	6.23	0.164	2.97	6.04	0.278	0.671	0.187	0.127	21.5	1.5	1250	2.77	2.07	12.8	0.218	1.21
NIF-4	**endmember**	**7380**	**2100**	**380**	**76**	**32.3**	**231**	**515**	**37.6**	**70.2**	**26.7**	**7.94**	**2210**	**130**	**21400**	**442**	**88.4**	**133**	**3.39**	**2.9**
	uncertainty of regression	391	112	20.6	4.19	1.74	13.1	27.7	2.03	3.81	1.47	0.421	118	6.87	1160	23.4	4.76	9.03	0.186	0.448
NIF-5	**endmember**	**677**	**100**	**72.5**	**12.2**	**9.67**	**68.8**	**133**	**5.17**	**16.4**	**8.46**	**2.19**	**510**	**26.9**	**20700**	**166**	**32.3**	**22**	**0.802**	**0.331**
	uncertainty of regression	33.3	5	3.7	0.6349	0.486	3.65	6.59	0.262	0.838	0.432	0.108	25	1.32	1050	8.15	1.64	1.63	0.0413	0.0831

Table 3

Table 3: Calculated endmember concentrations of REY in NIF-1, NIF-2, NIF-4, and NIF-5, concentrations in ng/l, ABSW: Ambient Bottom Sea Water

Element	56 CTD ABSW	NIF-2 (60 ROV-1B)	NIF-1 (27 ROV-14C)	NIF-4	NIF-5
Y	17.7	2960	620	2660	2190
La	2.4	5830	2220	3250	6260
Ce	0.547	9980	2970	6770	10400
Pr	0.476	1300	338	679	1110
Nd	2.02	5170	1260	2510	4010
Sm	0.408	1090	292	713	970
Eu	0.127	1150	303	688	711
Gd	0.721	1010	307	804	999
Tb	0.117	120	36.8	105	106
Dy	1.02	579	177	603	552
Ho	0.289	90.7	25.3	102	80.8
Er	1.04	206	49.1	262	203
Tm	-	-	-	-	-
Yb	1.02	114	22.3	170	119
Lu	0.155	12.8	2.36	20.2	13.2

Table 4

Table 4: Endmember fluid compositions of Nifonea vent fluids in comparison to other hydrotherr
EPR 9°N, (Von Damm, 2000), Main Endeavour Field (Seyfried et al., 2003), E9 Scotia Ridge (Ja
2007), TAG (Douville et al., 2002; Charlou et al., 1996; Metz and Trefry, 2000), Manus Basin (Cı
ELSC (Mottl et al., 2011), SW: seawater

		Nifonea	**E9 East Scotia Ridge**	**MEF JdFR**	**9°46' N EPR**	**5°S MAR**	**Manus Basin**
		NIF-5	***B&W***	***Sully***	***Aa2***	***Red Lion***	***Pacmanus F3*** *(dacite)*
mM	SO4	2.13	-	-	-	-	-
mM	H2S	6.68	9.5	20	66	-	18.8
°C	T	368	383	379	396	349	358
mM	Cl	25.1	98.2	39	30.5	552	562
mM	Br	0.0591	0.172	0.05	0.043	0.87	0.882
µM	B	1560	458	980	-	520	1610
mM	Si	5.32	8.19	2.9	3.8	21.8	12.2
nM	Ge	27.5	-	-	-	-	-
µM	Al	2.18	-	1.3	-	-	-
mM	Na	20.6	96	31.1	24.9	480	397.0
mM	K	0.375	6.53	1.94	0.624	19.8	76.1
µM	Li	2.17	122	30	15.6	1220	917
µM	Rb	0.0902	-	2	-	-	77
nM	Cs	0.485	64.5	25	-	-	2750
mM	Ca	5.29	6.68	1.85	1.45	18.6	22.3
µM	Sr	11.7	22.7	10	2.99	63.1	95.9
µM	Fe	677	800	400	722	803	11800
µM	Mn	100	199	90	102	730	3800
µM	Cu	9.67	160	12	-	209	138
µM	Zn	68.8	29	18	-	257	390
nM	Cd	133	-	25	-	-	480
nM	Ag	5.18	-	4	-	-	290
nM	Pb	510	-	100	-	-	18000
nM	As	20700	-	-	-	-	15800
nM	Mo	22.1	-	38	-	-	
nM	U	0.33	-	-	-	-	
nM	ΣREE	179	-	-	-	7.73	83.5
mM/mM	Na/Cl	0.821	0.978	0.797	0.816	0.87	-
mM/mM	K/Cl	0.015	0.0665	0.0497	0.0205	0.0359	0.135
µM/mM	Li/Cl	0.0865	1.24	0.769	0.511	2.21	1.63
mM/mM	Ca/Cl	0.211	0.068	0.0474	0.0475	0.0337	0.0397
µM/mM	Sr/Cl	0.46	0.231	0.256	0.098	0.114	-
µM/mM	B/Cl	62.3	4.66	25.1	-	0.942	-
µM/mM	Fe/Cl	27	8.15	10.3	23.7	1.45	21.0
µM/mM	Mn/Cl	3.98	2.03	2.31	3.34	1.32	6.76
µM/µM	Fe/Mn	6.77	4.02	4.44	7.08	1.1	3.11
µM/mM	Si/Cl	0.212	0.0834	0.0744	0.125	0.0395	-
µM/mM	H2S/Cl	266	96.7	513	2160	-	-
µM/mM	Cu/Cl	0.38	1.63	0.308	-	-	0.246
µM/mM	Zn/Cl	2.75	0.295	0.462	-	-	0.694

Table EA 2

Table EA 2: Element/Cl ratios, Fe/H2S, and Ge/Si ratios of Nifonea vent fluids and in calculated endmembers

Sample ID	Br/Cl	Na/Cl	K/Cl	Li/Cl	Rb/Cl	Cs/Cl	Ca/Cl	Sr/Cl	B/Cl	Fe/Cl	Mn/Cl	Fe/Mn	Si/Cl	As/Cl	Ge/Cl	Al/Cl	H2S/Cl	Cu/Cl	Zn/Cl	Pb/Cl	Tl/Cl	Ag/Cl	Ge/Si	Fe/H2S
	µM/mM	*mM/mM*	*mM/mM*	*µM/mM*	*nM/mM*	*nM/mM*	*mM/mM*	*µM/mM*	*µM/mM*	*µM/mM*	*µM/mM*	*µM/µM*	*mM/mM*	*µM/mM*	*nM/mM*	*µM/mM*	*µM/mM*	*µM/mM*	*µM/mM*	*nM/mM*	*nM/mM*	*nM/mM*	*nM/mM*	*µM/mM*
56 CTD 1900	1.48	0.87	0.0193	0.0486	2.73	0.00349	0.0191	0.167	0.769	8.26E-06	-	-	0.000187	4.35E-05	0.000732	0.000183	-	1.02E-05	0.000177	0.00196	8.07E-05	#VALUE!	3.91	-
27 ROV 14 KIPS A	1.52	0.846	0.0185	0.0489	-	-	0.025	0.164	1.33	-	-	-	0.00277	-	-	-	-	-	-	-	-	-	-	-
27 ROV 14 KIPS B	1.61	0.815	0.018	0.0575	3.05	0.0113	0.0584	0.189	5.21	5.16	2.35	2.2	0.0202	0.0432	0.0763	0.00665	-	0.0139	0.212	1.62	0.183	0.0165	3.77	-
27 ROV 14 KIPS C	1.56	0.845	0.0185	0.0575	3.08	0.0099	0.0484	0.184	4.37	4.56	2.13	2.14	0.0163	0.0384	0.0679	0.00484	-	0.0056	0.158	1.43	0.131	0.00715	4.17	-
66 ROV 1 KIPS B	1.51	0.859	0.0186	0.0521	3.02	0.00772	0.0317	0.172	2.3	-	-	-	0.00743	-	-	-	25.1	-	-	-	-	-	-	-
60 ROV 1 KIPS B	1.54	0.868	0.0194	0.0564	3.24	0.00807	0.0323	0.172	2.61	0.303	0.578	0.525	0.0145	0.0264	0.0686	0.0733	26.4	0.00358	0.0659	0.483	0.0304	0.00601	4.72	11.5
60 ROV 1 KIPS C	1.5	0.853	0.0188	0.0504	2.84	0.00504	0.0247	0.166	1.27	0.1	0.196	0.513	0.00545	0.0068	0.0268	0.0122	7.36	0.00145	0.0281	0.155	0.00732	0.00158	4.92	13.6
60 ROV 1 KIPS D	1.54	0.866	0.0192	0.0553	-	-	0.0257	0.168	1.33	-	-	-	0.00583	-	-	-	-	-	-	-	-	-	-	-
66 ROV 6 KIPS D	1.5	0.854	0.0186	0.0487	2.75	0.00369	0.0212	0.16	1.2	0.297	0.115	2.59	0.00354	0.000421	0.0125	0.000583	3.49	7.25E-06	0.0105	0.0941	0.00668	#VALUE!	3.54	85.0
77 ROV 6 KIPS A	1.49	0.75	0.0186	0.0876	3.41	0.0229	0.0829	0.189	3.35	15.6	4.44	3.51	0.012	0.0453	0.0688	0.00929	13.8	0.0682	0.488	4.68	0.274	0.0794	5.72	1130
77 ROV 10 KIPS B	1.8	0.852	0.0177	0.0627	3.05	0.00936	0.0904	0.278	23.6	10	1.48	6.77	0.0788	0.306	0.407	0.0322	98.9	0.143	1.02	7.54	0.399	0.0766	5.16	101
66 ROV 3 KIPS C	1.52	0.845	0.0188	0.0529	2.89	0.00355	0.0285	0.164	1.16	1.79	0.56	3.19	0.00211	0.00411	0.0112	0.00134	3.31	0.00246	0.0308	0.298	0.0177	0.00246	5.3	540
66 ROV 5 NISKIN	1.48	0.848	0.0185	0.047	2.62	0.00376	0.0204	0.159	0.804	0.24	0.0749	3.21	0.000418	0.00124	0.00202	0.000503	-	0.00119	0.0106	0.12	0.00714	0.00114	4.82	-

Endmembers

	Br/Cl	Na/Cl	K/Cl	Li/Cl	Rb/Cl	Cs/Cl	Ca/Cl	Sr/Cl	B/Cl	Fe/Cl	Mn/Cl	Fe/Mn	Si/Cl	As/Cl	Ge/Cl	Al/Cl	H2S/Cl	Cu/Cl	Zn/Cl	Pb/Cl	Tl/Cl	Ag/Cl	Ge/Si	Fe/H2S
	µM/mM	*mM/mM*	*mM/mM*	*µM/mM*	*nM/mM*	*nM/mM*	*mM/mM*	*µM/mM*	*µM/mM*	*µM/mM*	*µM/mM*	*µM/µM*	*mM/mM*	*µM/mM*	*nM/mM*	*µM/mM*	*µM/mM*	*µM/mM*	*µM/mM*	*nM/mM*	*nM/mM*	*nM/mM*	*nM/mM*	*µM/mM*
NIF-1	1.93	0.712	0.0149	0.0886	4.43	0.0371	0.169	0.256	18.6	21.6	9.93	2.18	0.0805	0.18	0.317	0.0254	191	0.0432	0.818	6.74	0.694	0.0524	3.94	0.113
NIF-2	2.05	0.848	0.0203	0.118	7.02	0.0432	0.135	0.211	16.7	2.62	4.99	0.524	0.125	0.227	0.589	0.626	227	0.031	0.571	4.15	0.26	0.0517	4.71	0.0115
NIF-4	**1.49**	**0.651**	**0.018**	**0.12**	**3.97**	**0.0389**	**0.136**	**0.206**	**5.49**	**28.5**	**8.11**	**3.51**	**0.0218**	**0.0827**	**0.125**	**0.017**	**25.2**	**0.125**	**0.891**	**8.54**	**0.501**	**0.145**	**5.73**	**1.13**
NIF-5	**2.35**	**0.821**	**0.0151**	**0.0865**	**3.57**	**0.0193**	**0.211**	**0.466**	**62.2**	**27**	**3.98**	**6.77**	**0.212**	**0.825**	**1.1**	**0.0869**	**266**	**0.385**	**2.74**	**20.3**	**1.07**	**0.206**	**5.17**	**0.101**
Element/Cl_{NIF-5} / Element/Cl_{NIF-4}	1.6	1.3	0.8	0.7	0.9	0.5	1.6	2.3	11.3	0.9	0.5	1.9	9.7	10.0	8.8	5.1	10.6	3.1	3.1	2.4	2.1	1.4		

Figures

Figure 1: (a) Bathymetric map of the Coriolis Troughs as originally published in Anderson et al. (2016), inlay map: Vanuatu Island Arc with the recently active central chain, and the location of the Nifonea vent field in the Vate Trough (black star), (b) Nifonea vent field with sample locations and maximum measured temperatures.

Figure 2: Vent sites in the Nifonea hydrothermal field: (A) Black smoker NIF-1 in about 1862 m, 2.5 m tall, T >>250°C (samples 27 ROV-14); B) black fluid at NIF-1 site, chimney re-grown within 7 days, 2 phase venting observed, 20–30 cm tall, 107°C & 132°C measured, 1862 m (sample 66 ROV-1); (C) Clear fluid venting directly from the seafloor – NIF-2, 2 phase venting observed, 0–2 cm tall, 345 °C, 1873 m (60 ROV-1); D) black fluid, 2 phase venting observed, ~1 m tall, ~1862 m (not sampled, near NIF-3); (E) black fluid at site NIF-4, vigorous 2 phase venting observed, 30–40 cm, 368 C, 1862 m (sample 77 ROV-6); (F) grey to black fluid at NIF-5, 2 phase venting observed, <1 m tall, 368 C, 1862 m (sample 77 ROV-10).

Figure 3: Measured element concentrations versus measured Mg concentrations for individual fluid samples of vent sites NIF-1, NIF-2, NIF-3, NIF-4 and NIF-5. Trend line for NIF-2 only based on one fluid sample, see text for discussion.

Figure 4: End-member Cl-normalized element concentrations vs. 1/Cl for individual sites.

Figure 5: Chondrite-normalized rare earth element and Y distribution in Nifonea vent fluids. Literature data for high-temperature hydrothermal fluids from sediment-starved Mid-Ocean Ridge and back –arc hydrothermal systems in grey (Douville et al., 1999; Mitra et al., 1994; Bau and Dulski, 1999; James et al., 1995; Cole et al., 2014; Craddock et al., 2010), acid-sulfide fluids are excluded from this compilation.

Figure 6: Temperature-pressure diagram for the system NaCl-H_2O with the isosalinity liquid-vapor two-phase boundary of seawater (3.2 wt% NaCl).

Figure 7: End-member (EM) concentrations vs. corresponding end-member Cl concentratios for individual vent sites.

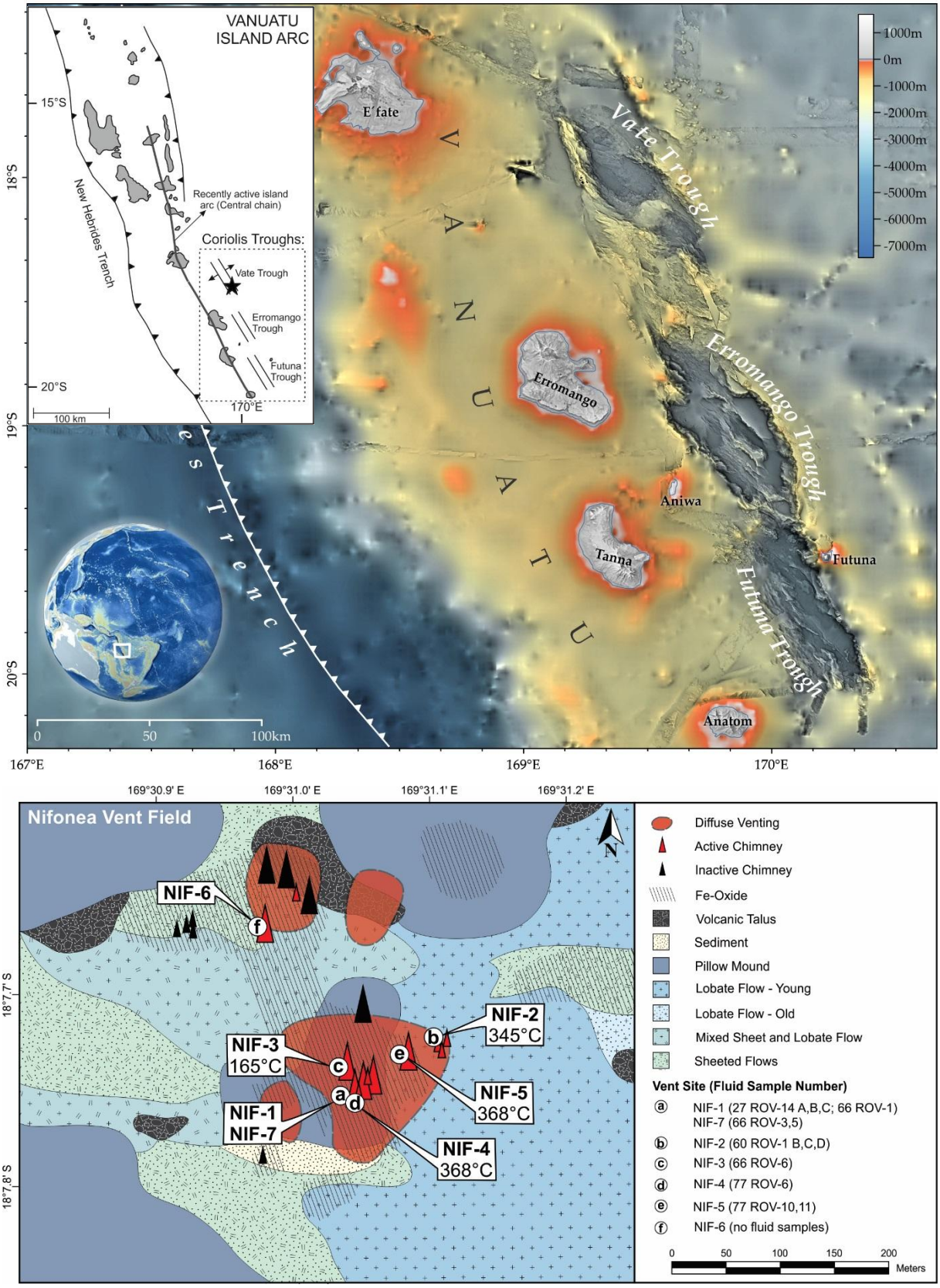

Figures 1a and 1b

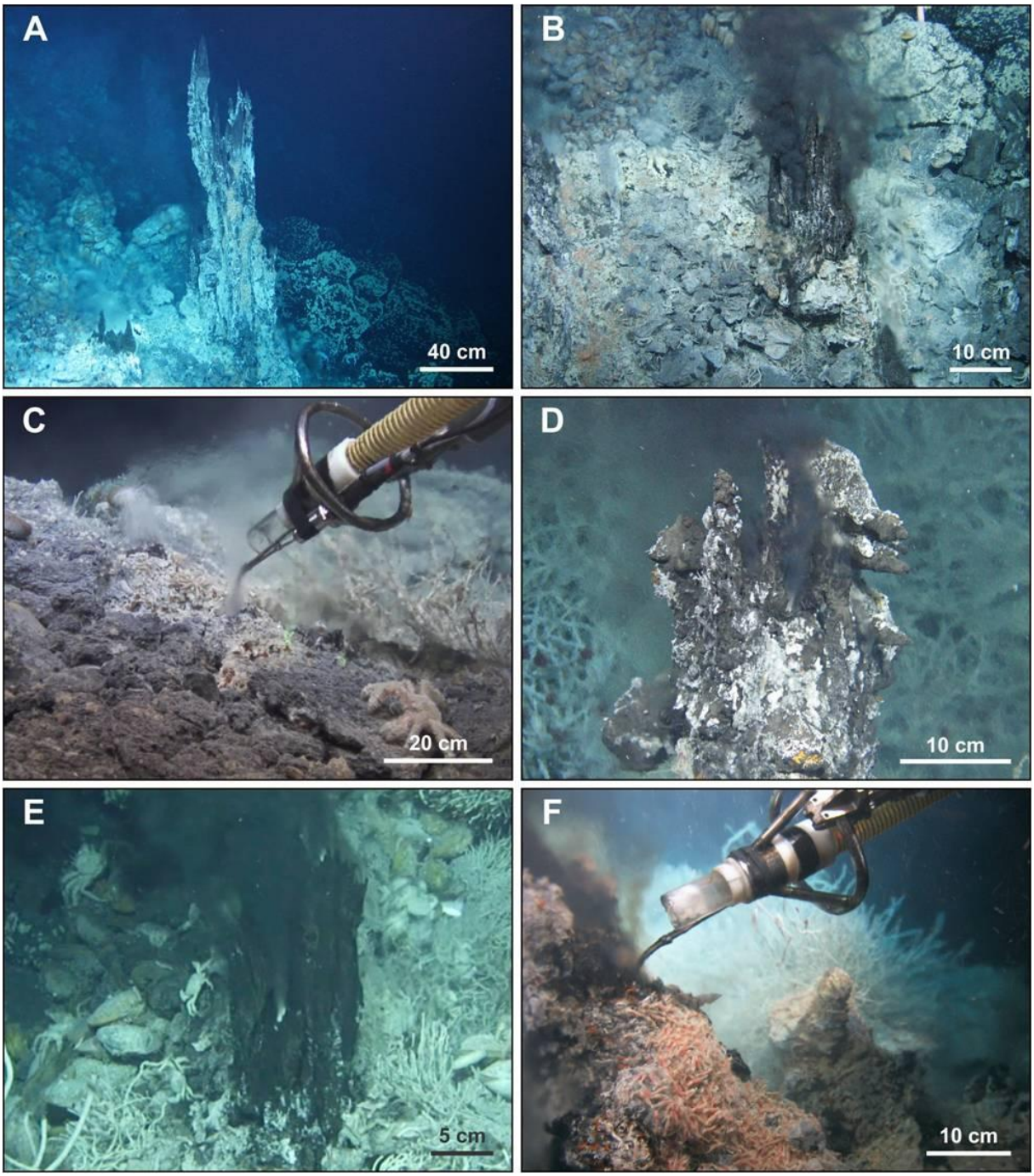

Figure 2

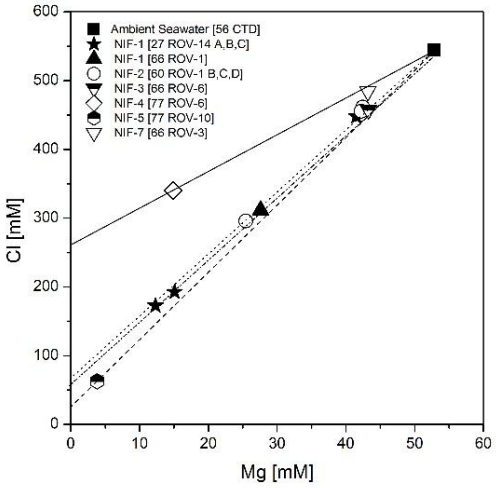
Ambient Seawater [56 CTD]
NIF-1 [27 ROV-14 A,B,C]
NIF-1 [66 ROV-1]
NIF-2 [60 ROV-1 B,C,D]
NIF-3 [66 ROV-6]
NIF-4 [77 ROV-6]
NIF-5 [77 ROV-10]
NIF-7 [66 ROV-3]
Cl [mM]
Mg [mM]

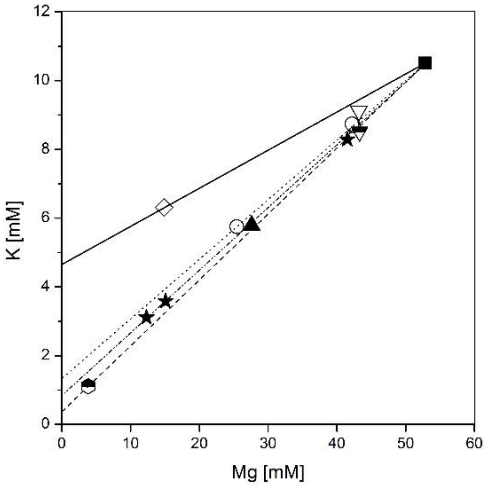
K [mM]
Mg [mM]

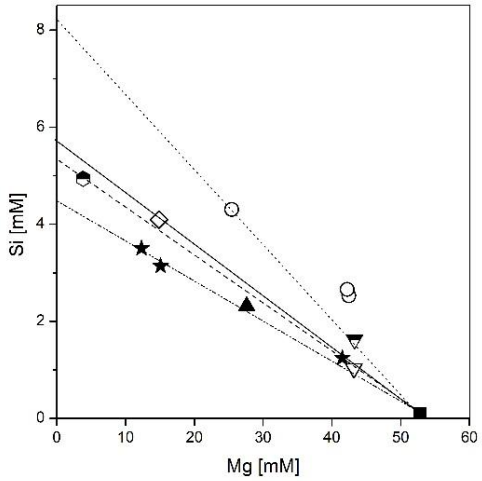
Si [mM]
Mg [mM]

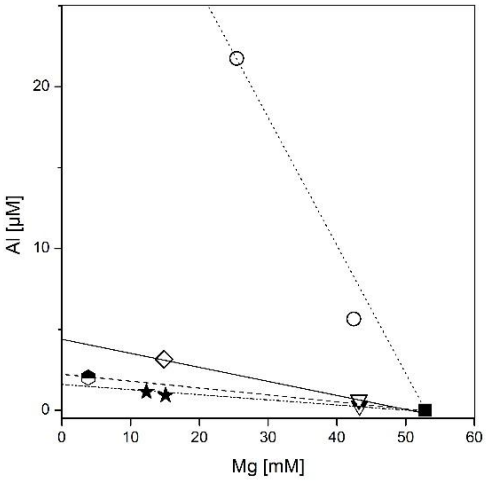
Al [µM]
Mg [mM]

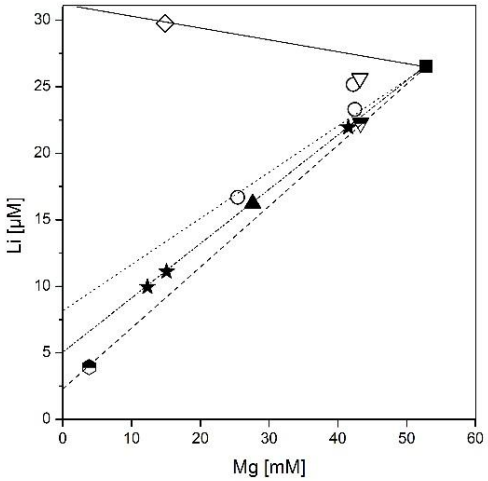
Li [µM]
Mg [mM]

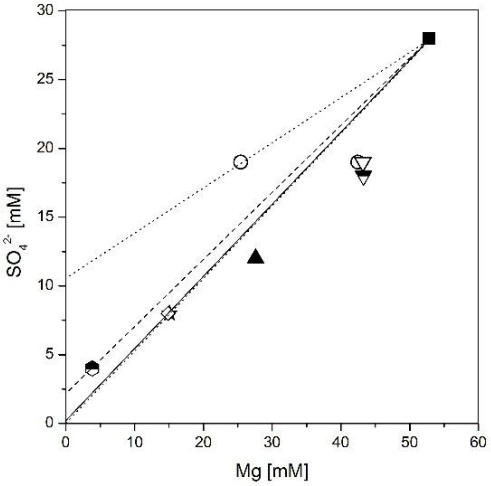
SO4 2- [mM]
Mg [mM]

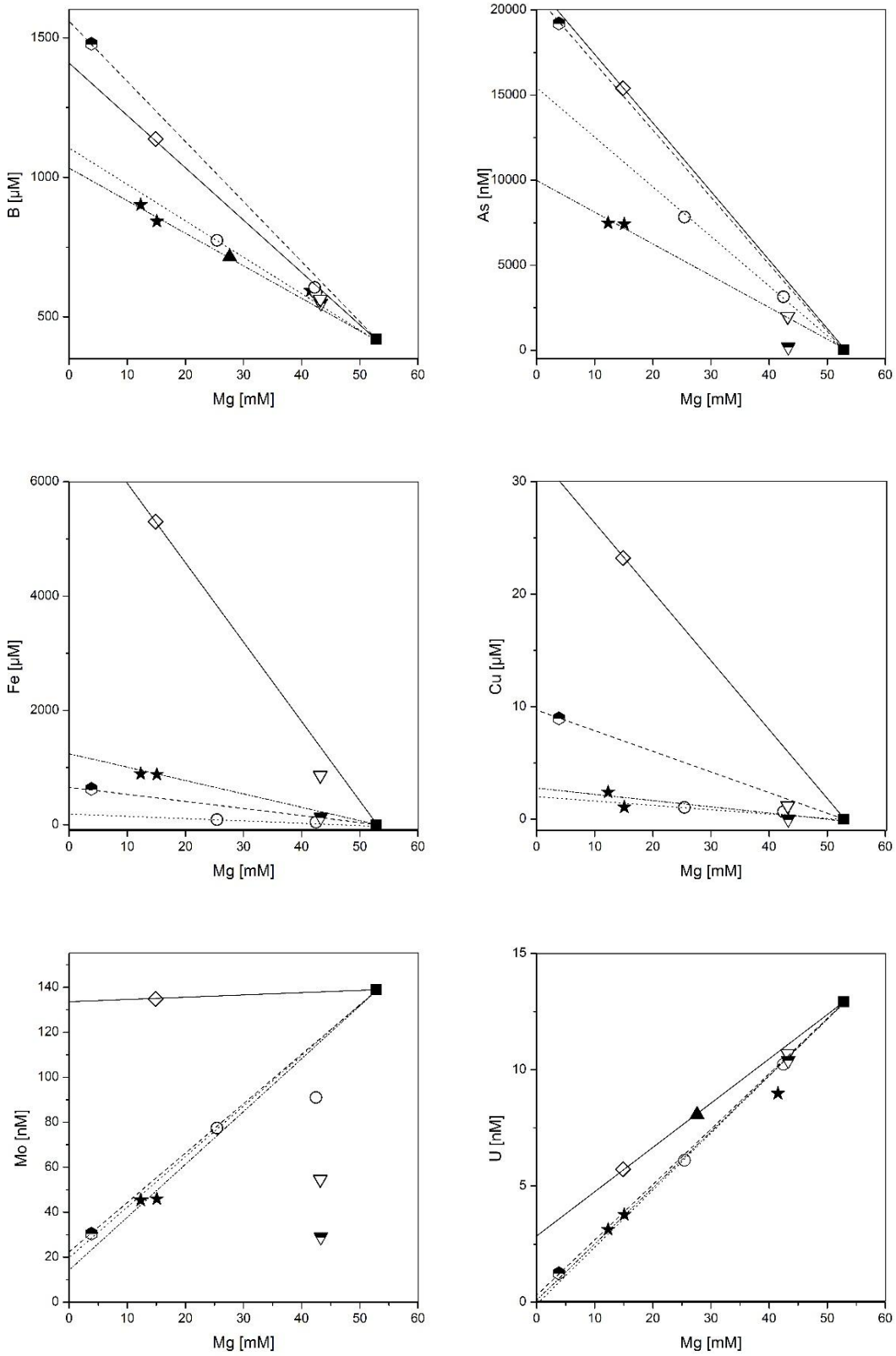

Figure3

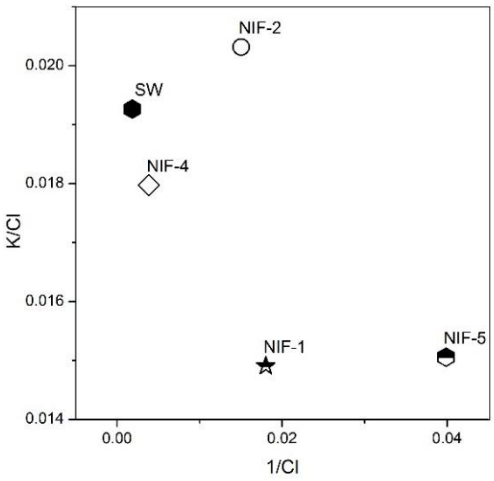
NIF-2
SW
NIF-4
NIF-1
NIF-5
K/Cl
1/Cl
0.020
0.018
0.016
0.014
0.00
0.02
0.04

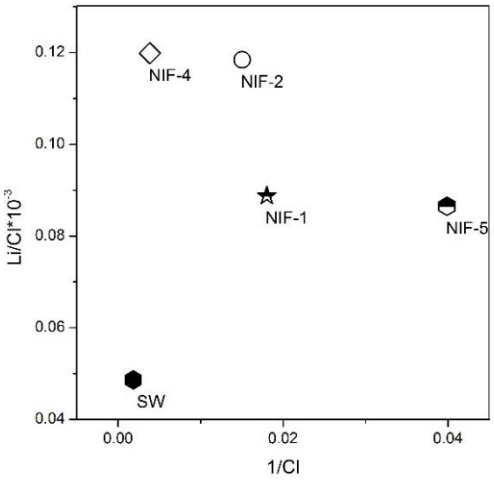
NIF-4
NIF-2
NIF-1
NIF-5
SW
Li/Cl*10-3
1/Cl
0.12
0.10
0.08
0.06
0.04
0.00
0.02
0.04

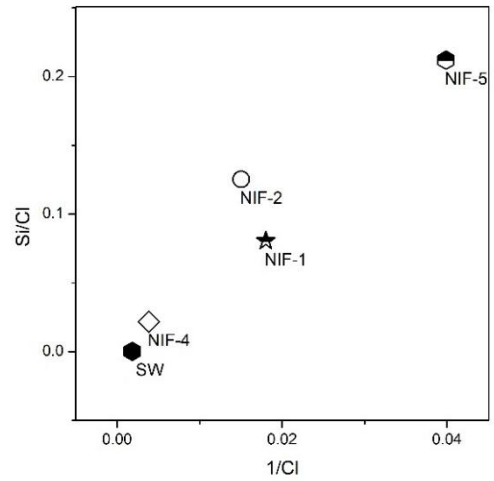
NIF-5
NIF-2
NIF-1
NIF-4
SW
Si/Cl
1/Cl
0.2
0.1
0.0
0.00
0.02
0.04

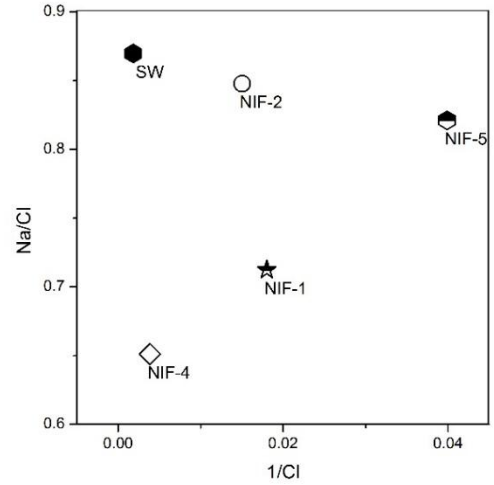
SW
NIF-2
NIF-5
NIF-1
NIF-4
Na/Cl
1/Cl
0.9
0.8
0.7
0.6
0.00
0.02
0.04

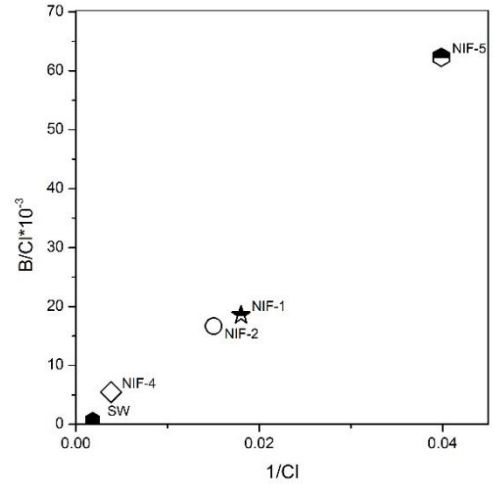
NIF-5
NIF-1
NIF-2
NIF-4
SW
B/Cl*10-3
1/Cl
70
60
50
40
30
20
10
0
0.00
0.02
0.04

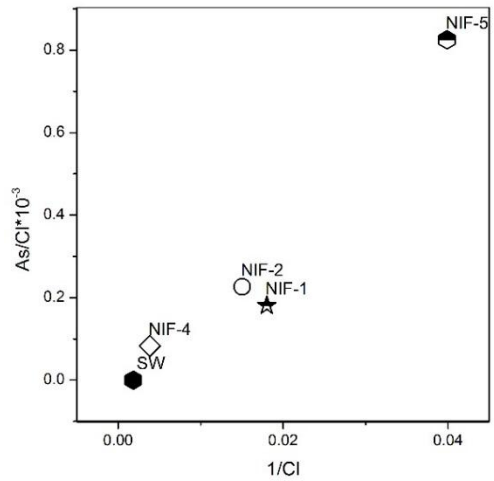
NIF-5
NIF-2
NIF-1
NIF-4
SW
As/Cl*10-3
1/Cl
0.8
0.6
0.4
0.2
0.0
0.00
0.02
0.04

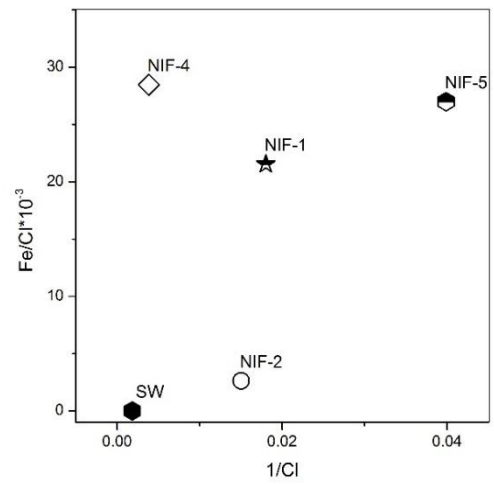
NIF-4
NIF-5
NIF-1
NIF-2
SW
Fe/Cl*10-3
1/Cl
0
10
20
30
0.00
0.02
0.04

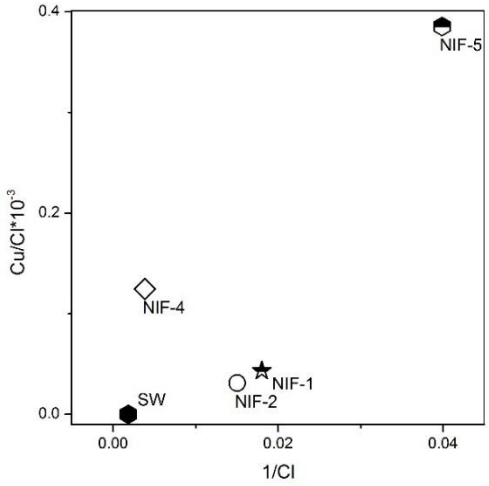
NIF-5
NIF-4
NIF-1
NIF-2
SW
Cu/Cl*10-3
1/Cl
0.0
0.2
0.4
0.00
0.02
0.04

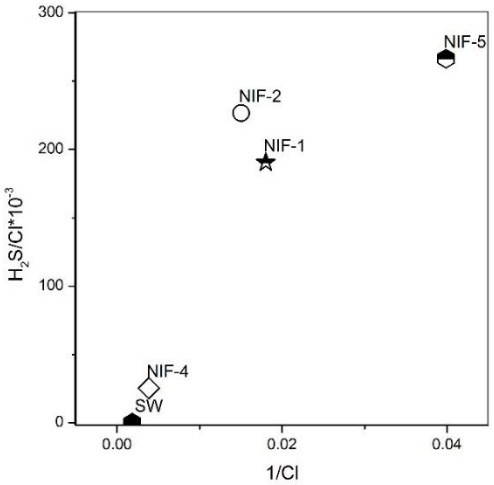
NIF-5
NIF-2
NIF-1
NIF-4
SW
H2S/Cl*10-3
1/Cl
0
100
200
300
0.00
0.02
0.04

Figure 4:

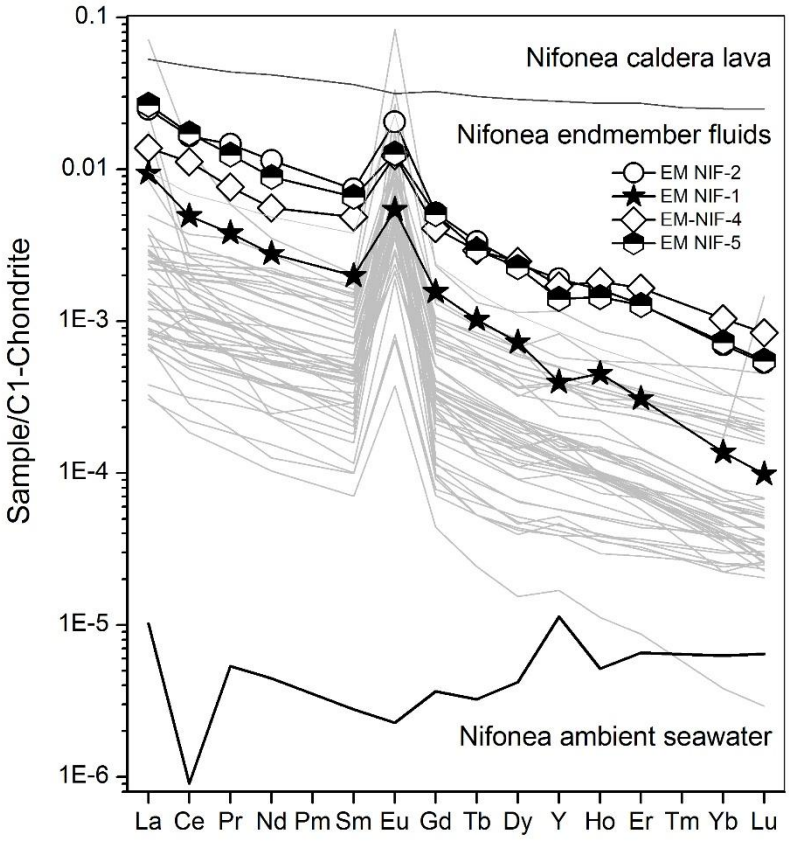

Figure 5:

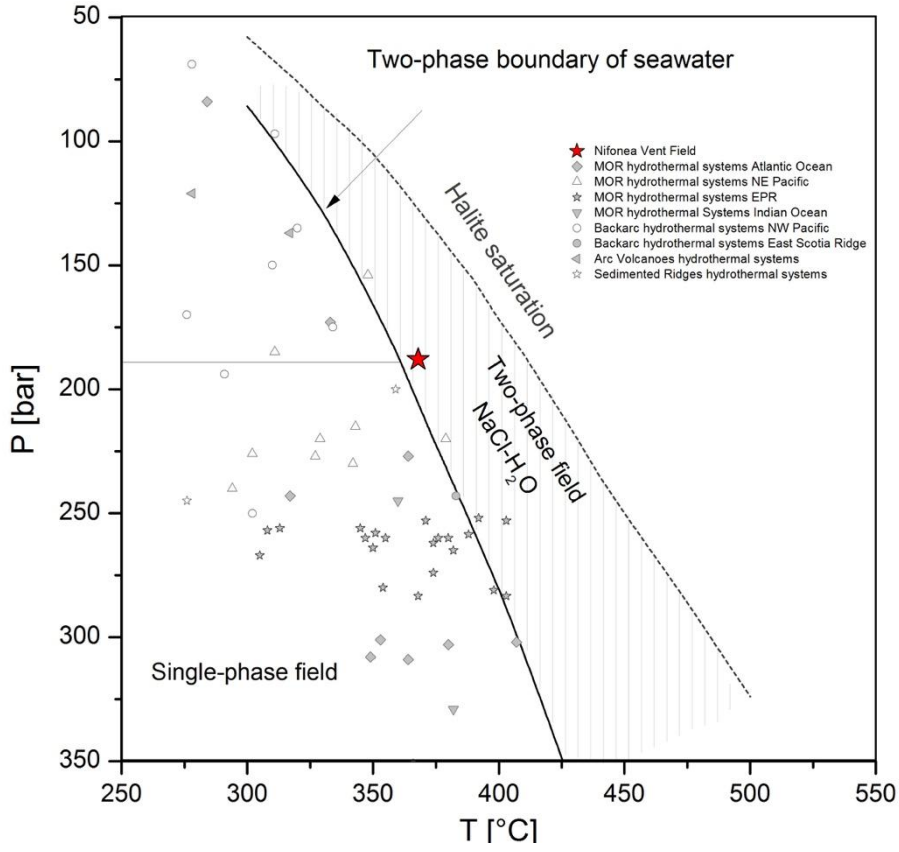

Figure 6

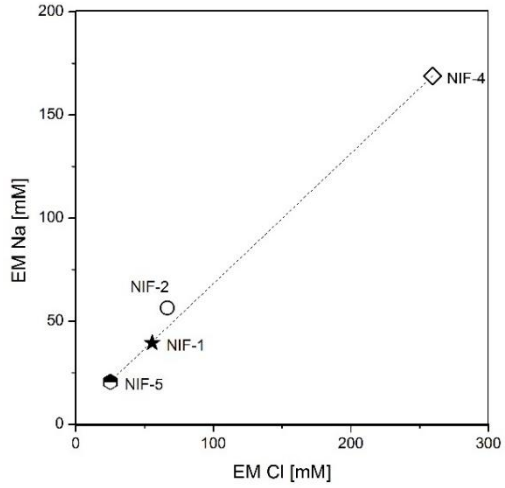
EM Na [mM]
EM Cl [mM]
NIF-4
NIF-2
NIF-1
NIF-5

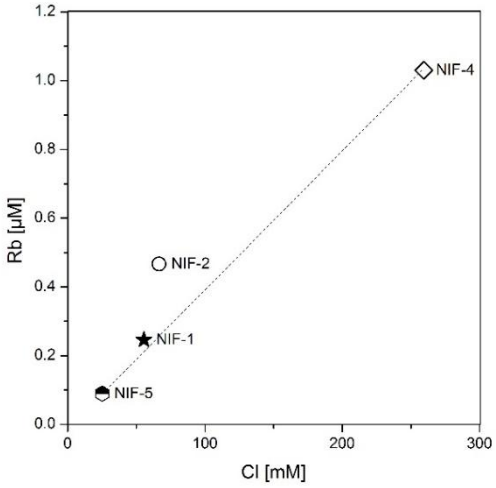
Rb [µM]
Cl [mM]
NIF-4
NIF-2
NIF-1
NIF-5

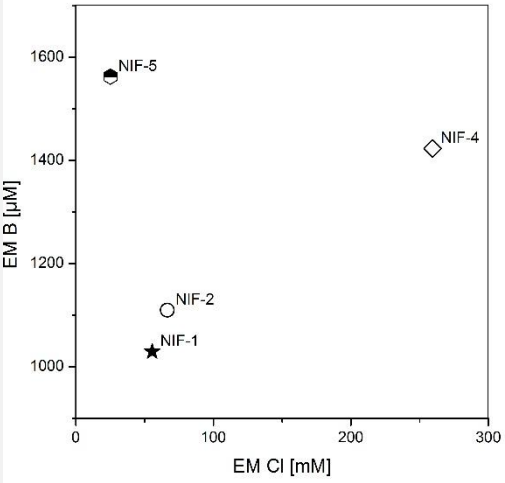
EM B [µM]
EM Cl [mM]
NIF-5
NIF-4
NIF-2
NIF-1

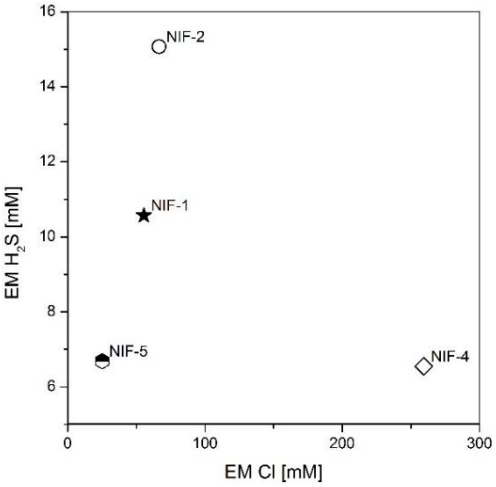
EM H2S [mM]
EM Cl [mM]
NIF-2
NIF-1
NIF-5
NIF-4

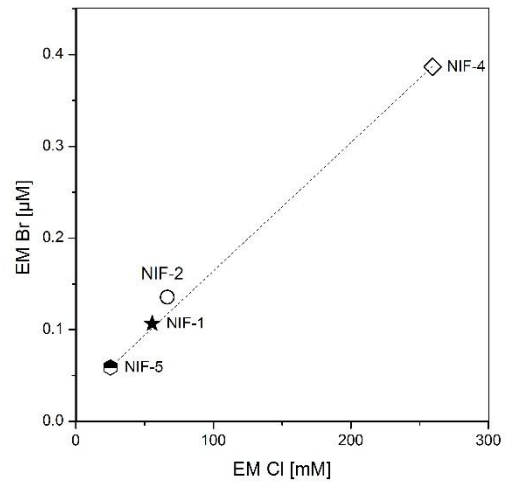
EM Br [µM]
EM Cl [mM]
NIF-4
NIF-2
NIF-1
NIF-5

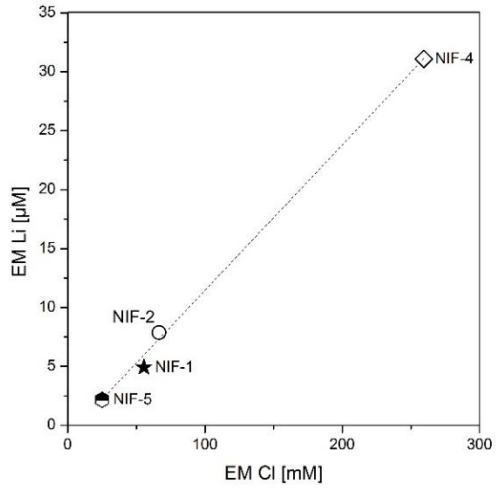
EM Li [µM]
EM Cl [mM]
NIF-4
NIF-2
NIF-1
NIF-5

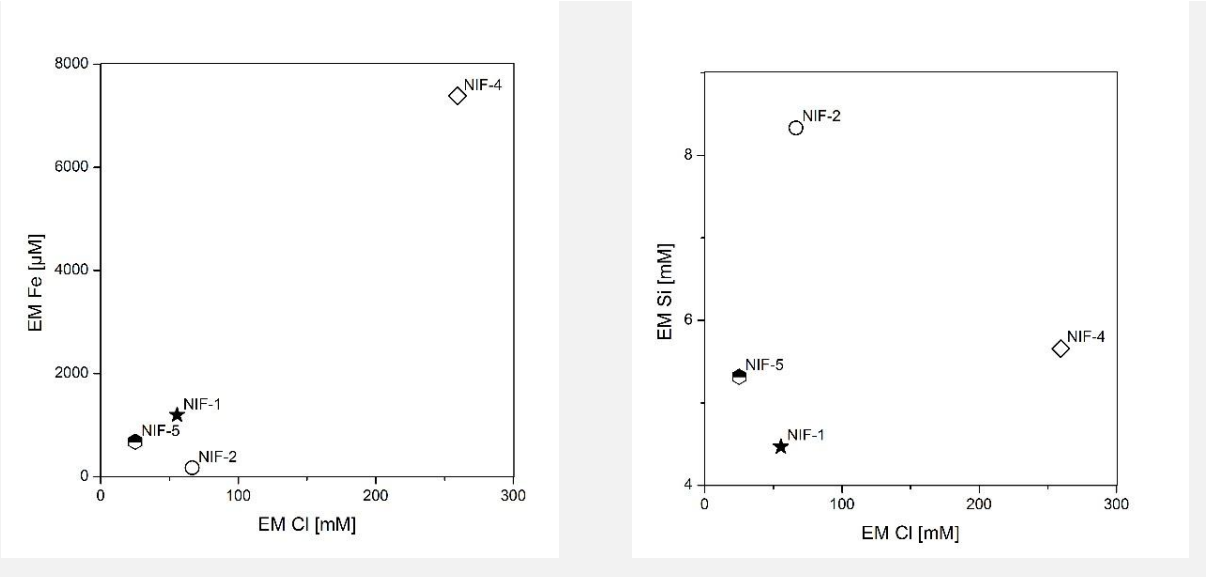
8000
6000
4000
2000
0
EM Fe [µM]
NIF-4
NIF-1
NIF-5
NIF-2
0
100
200
300
EM Cl [mM]
8
6
4
EM Si [mM]
NIF-2
NIF-4
NIF-5
NIF-1
0
100
200
300
EM Cl [mM]

Figure 7